JGR Oceans

RESEARCH ARTICLE
10.1029/2020JC017025

The Transfer of Antarctic Circumpolar Waters to the Western South Atlantic Ocean

Anna Olivé Abelló[1], Josep L. Pelegrí[1], Francisco J. Machín[2], and Ignasi Vallès-Casanova[1]

[1]Departament d'Oceanografia Física i Tecnològica, Institut de Ciències del Mar, CSIC, Unidad Asociada ULPGC-CSIC, Barcelona, Spain, [2]Departamento de Física Aplicada, Universidad de Las Palmas de Gran Canaria, Las Palmas de Gran Canaria, Spain

Key Points:

- We use Argo float data to calculate mean water transports into and out of the Scotia Sea and assess volume balances for fully sampled layers
- Our study reveals high seasonal and moderate interannual water-transport variability, with substantial interannual changes in composition
- The water transports and float trajectories expose the influence of frontal systems and bottom topography, with high cross-frontal exchange

Supporting Information:

Supporting Information may be found in the online version of this article.

Correspondence to:

A. Olivé Abelló and J. L. Pelegrí,
aolive@icm.csic.es;
pelegri@icm.csic.es

Citation:

Olivé Abelló, A., Pelegrí, J. L., Machín, F. J., & Vallès-Casanova, I. (2021). The transfer of Antarctic circumpolar waters to the western South Atlantic Ocean. *Journal of Geophysical Research: Oceans*, *126*, e2020JC017025. https://doi.org/10.1029/2020JC017025

Received 30 NOV 2020
Accepted 23 JUN 2021

Abstract Southern Ocean waters enter the South Atlantic Ocean through the Scotia Sea along pathways constrained by the bathymetry of the northern Scotia Sea passages. We use the Argo profiling-float data set to calculate the water transports in and out of the region, focusing on the water balances down to the deepest isoneutral sampled in all passages ($\gamma^n = 28.0$ kg m^{-3}, located between about 500 and 2,000 m in the Drake Passage and even shallower in the Northern Passages). Down to this reference level, the water inflow through the Drake Passage is 140.8 ± 7.4 Sv and the water outflow through the deeper portions of the Northern Passages is 115.9 ± 8.3 Sv, implying a leakage of about 25 ± 11.1 Sv over topography shallower than 1,000 m. Below the reference isoneutral and down to 2,000 m, an additional 23.4 Sv enter through the Drake Passage; when added to reported inputs of about 20 Sv through the South Scotia Ridge, this accounts well for the observed 43.4 Sv outflow–from 28.0 kg m^{-3} to 2,000 m–through the Northern Passages. Relative to the 2,000 m reference level, the mean barotropic contribution always represents over half the total transports. We also observe substantial seasonal and moderate interannual variations in the water transports and composition (peak differences occur seasonally in the Drake Passage, with a range of 111–174 Sv), associated with changes in water exchange across the frontal systems. Two independent measures set the water mean-residence time in the Scotia Sea at about 6–8 months.

Plain Language Summary The Scotia Sea is the entryway for Southern Ocean waters into the western South Atlantic Ocean, with waters entering through the Drake Passage (the Southern Ocean narrowest conduit) and exiting through several deep northern passages. Most of this transit water follows convoluted bands characterized by sharp horizontal gradients in water properties (frontal systems). We use the large set of profiles of temperature and salinity from the Argo network of drifting ocean profilers to measure the amount, characteristics, and pathways of those waters entering and leaving the Scotia Sea down to 2,000 m, as well as to assess their seasonal and interannual variability. This data set allows us to explore the water transports and transformations down to a certain ocean density level that is well sampled within all passages. Down to this level, about 141 million cubic meters per second (Sverdrups) enter through the Drake Passage, and 116 Sverdrups eventually exit through the deeper portions of the Northern Passages. Our calculations also reveal variations in water transport at interannual scales, although these are fairly small compared with variability within a year. We also show that most water parcels take about 6–8 months to travel the Scotia Sea along pathways that often cross the frontal systems.

1. Introduction

The Antarctic Circumpolar Current (ACC) constitutes the skeleton of the global overturning circulation, as it exchanges heat, mass, and freshwater between the Pacific, Atlantic, and Indian oceans (Rintoul & Naveira Garabato, 2013). The persistent westerly wind field around Antarctica is the main forcing mechanism responsible for the eastward direction and predominantly barotropic structure of the ACC, although its path is largely constrained by bathymetric features. However, the ACC does not flow as a single barotropic jet; instead, it exhibits a complex structure of frontal systems that merge and diverge along the circumpolar path, as reflected from the three-dimensional distribution of temperature, salinity, and dissolved oxygen (Kim & Orsi, 2014; Meredith et al., 2003; Orsi et al., 1995; Sokolov & Rintoul, 2007).

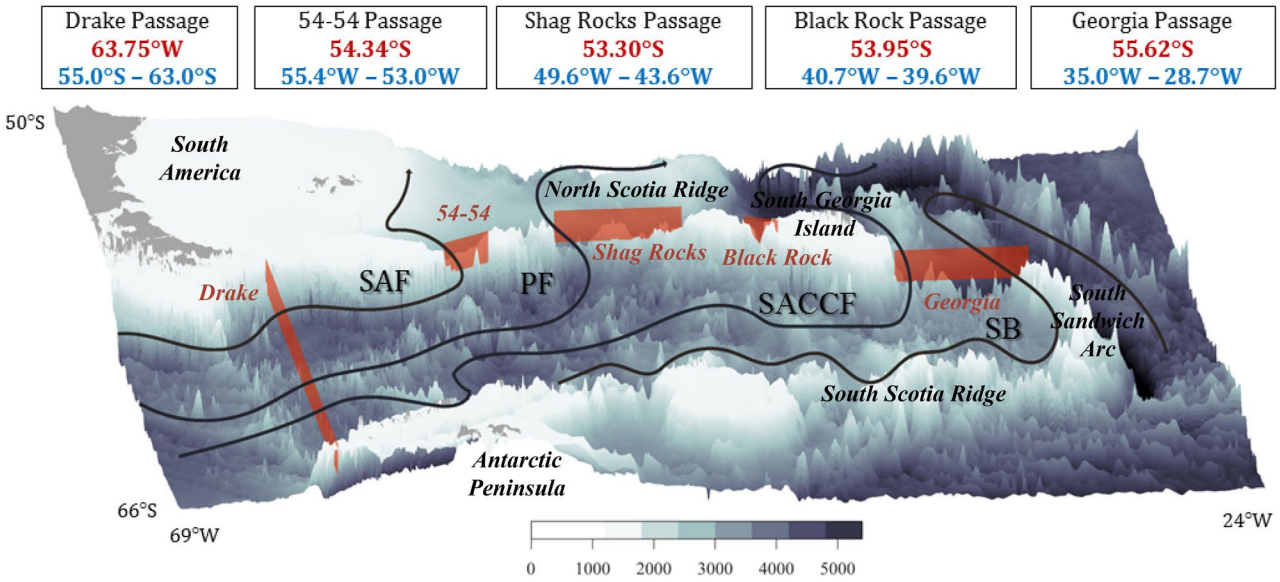

Figure 1. Bathymetry and main passages in the Scotia Sea, from west to east: Drake, 54–54, Shag Rocks, Black Rock, and Georgia. The red bands indicate the location of the sections used in this study to characterize these passages. The surface position of the principal fronts is shown schematically: Subantarctic Front (SAF), Polar Front (PF), Southern Antarctic Circumpolar Current Front (SACCF), and the Southern Boundary (SB).

A suitable location to measure the transport of the ACC is the latitudinally restricted Drake Passage. As part of the intensive measurements performed in the 1970s and 1980s during the International Southern Ocean Studies program, Whitworth and Peterson (1985) obtained the first ACC transport estimate, 134 Sv (1 Sv ≡ 10^6 m^3 s^{-1}). Later estimates, ranging between 130 and 170 Sv, included those obtained by Naveira Garabato et al. (2002, 2003), Orsi et al. (1995) and Sokolov and Rintoul (2009a, 2009b). More recent studies have found transports to be as large as 173 Sv (Chidichimo et al., 2014; Donohue et al., 2016) and 175 Sv (Colin de Verdière & Ollitrault, 2016).

After crossing the Drake Passage, the ACC enters the Scotia Sea, a semi-enclosed basin bound by submarine ridge systems and island arcs (Figure 1). The northern boundary is the North Scotia Ridge, a 2,000 km submarine arc with several deep passages, which stretches between the southern tip of South America and the South Georgia Island, and the eastern boundary is the South Sandwich Arc, which has much shallower passages. To the south is the South Scotia Ridge, which is the tectonic extension of the Antarctica Peninsula. The bulk of the water transport into the Scotia Sea is carried out by the jets associated with the Subantarctic Front (SAF) and the Polar Front (PF) (Orsi et al., 1995), which veer northward to exit through the passages in the North Scotia Ridge system (Smith et al., 2010). The remaining ACC water flows eastward through the Scotia Sea associated with the southern ACC Front (SACCF) and the Southern Boundary (SB) system, before exiting through the Georgia Passage, located east of South Georgia Island.

Several authors have explored how the ACC water masses leave the Scotia Sea through the topographic features along its boundary (e.g., Naveira Garabato et al., 2002, 2003; Thompson & Sallée, 2012). Smith et al. (2010) determined that the total net volume transport associated with the SAF and PF systems over the North Scotia Ridge is 117 ± 10 Sv. Meredith et al. (2003) and Thorpe et al. (2002) explored the characteristics and temporal variability of the SACCF north of the South Georgia Island. In contrast, along the South Scotia Ridge, the presence of the Weddell-Scotia confluence acts as a barrier to water exchange between the Scotia Sea and the Weddell Gyre (Locarnini et al., 1993; Naveira Garabato et al., 2003).

The spatial pathways and temporal variability of the water fluxes through the Scotia Sea remain open questions. In this study, we use the Argo float data set to document these fluxes, with special attention to the role of cross-frontal exchange. In Section 2, we present the study area, the float data set, and the data processing details. In Section 3, we show how we use the float data to develop hydrographic sections and reference velocities, which are used to obtain the transports. In Section 4, we explore how these transports are associated

with the different fronts, their interannual and seasonal variability, and how they evolved during one and a half decades of the Argo data set. We conclude in Section 5 with some remarks about what we know and what yet remains unknown regarding the ACC structure across the passages bordering the Scotia Sea.

2. Material and Methods

2.1. Study Area

There are three main deep passages along the North Scotia Ridge (Figure 1), from west to east: the 54–54 Passage, the relatively deep and wide Shag Rocks Passage, and the narrow Black Rock Passage. Further east, between South Georgia Island (the easternmost landmass of the North Scotia Ridge) and the South Sandwich Arc, the Georgia Passage (35.0°W–28.7°W) is the deepest passage out of the Scotia Sea (3,200 m). Hereafter, we will refer to these four passages (the three North Scotia Ridge Passages and the Georgia Passage) as the Northern Passages. There are some other significant passages in the South Sandwich Arc and the South Scotia Ridge, but we chose not to consider them in this study, as justified in the next subsection.

2.2. Argo Floats

The Argo program, which started in 1999 and became fully operational in 2007, provides a valuable set of observations to investigate the hydrography of the upper 2,000 m of the water column, study the preferential pathways of intermediate waters, and explore the temporal variability of water transports and pathways. For our study, we have used all Argo float data (flagged as good) with a 1,000 m parking depth, from January, 2002 to December, 2018.

In order to construct average hydrographic sections, from the sea surface down to 2,000 m, we have used all float conductivity-temperature-depth (CTD) casts in a 50 km wide band, adjacent to the prescribed location of each passage's section (Figure 1). The total number of CTD casts used within these 50 km wide passages is 527, distributed as follow: 221 profiles in Drake Passage, 211 profiles in the North Scotia Ridge passages (76, 116, and 19 profiles for the 54–54, Shag Rocks and Black Rock Passages, respectively), and 95 profiles in Georgia Passage. During the entire period, a few floats recirculated within the Drake and Northern Passages, no floats were found along the South Sandwich Arc, and only three floats crossed the South Scotia Ridge. Therefore, we cannot estimate the transports through the passages in these eastern and southern arcs. Instead, we assume that the amount of ACC water crossing the eastern and southern boundaries of the Scotia Sea is small and will use previous reports for these regions (Naveira Garabato et al., 2003; Palmer et al., 2012; Thorpe et al., 2002) for drawing our final conclusions.

The number of floats that crossed the Drake Passage eastward is 198. However, in order to obtain the 1,000 m reference velocities, we only used those floats (177) that had a 10 days cycle and a parking depth near 1,000 m. Of these 1,000 m floats, 130 exited the Scotia Sea through the North Scotia Ridge passages (54, 66, and 10 through the 54–54, Shag Rocks and Black Rock Passages, respectively) and 40 through the Georgia Passage. The difference between the number of 1,000 m parking-depth floats entering the Drake Passage and exiting the Northern Passages (177 vs. 170) comes from 3 floats that exited through the South Scotia Ridge and 4 floats that either expired within the Scotia Sea or had not yet exited the region by December, 2018. Finally, in order to track the number of floats associated with each front and to obtain a mean water residence time within the Scotia Sea, we used 187 floats that were parked at 1,000 m, were released at least 30 days prior to reaching the Drake Passage, and crossed the entire Scotia Sea.

2.3. Data Processing

All float profiles measured near the sections (within the 50 km bands) are used to build the mean potential temperature and salinity vertical sections. These data are vertically interpolated at 10 dbar and horizontally gridded every 25 km, and further smoothed with a low-pass moving horizontal filter of 7 points, leading to an effective horizontal resolution of about 150 km. The neutral density and dynamic height anomaly (referenced to the 1,000 dbar level, matching with the parking depth for the selected Argo floats) are calculated at each grid point, and the relative geostrophic velocities are calculated at the central position between grid points using the thermal wind equation.

Table 1
Neutral Density Definitions for Water Masses in the Scotia Sea

Water mass	Acronym	Neutral density layer (kg m^{-3})
Subantarctic Surface Water	SASW	$\gamma^n < 26.90$
Subantarctic Mode Water	SAMW	$26.90 < \gamma^n < 27.18$
Antarctic Surface Water / Antarctic Intermediate Water	AASW/AAIW	$27.18 < \gamma^n < 27.55$
Upper Circumpolar Deep Water	UCDW	$27.55 < \gamma^n < 28.00$
Lower Circumpolar Deep Water	LCDW	$28.00 < \gamma^n < 28.26$
Weddell Sea Deep Water	WSDW	$28.26 < \gamma^n < 28.40$

The 1,000 m reference velocities are calculated directly from the distance between the location of the first fix position after the float's arrival to the sea surface and the last surface fix position preceding the previous profile, divided by the time separation of about 10 days (Lebedev et al., 2007; Ollitrault & Rannou, 2013; Rosell-Fieschi et al., 2015; Yoshinari et al., 2006). This is done for the fixings before and after crossing the nominal line defining each passage (Figure 1). The velocity error depends on the vertical shear and the duration of the float's vertical excursion and time spent at the sea surface. At the beginning of the Argo program, a float had to spend several hours at the surface in order to transmit the positioning and CTD data, usually spending more than 18 h away from its parking depth. However, recent changes in the transmitting technology allow sending these data in much less time, about 20 min, which reduces the errors associated with the calculation of the reference velocity.

The float positions allow estimating the 1,000 m velocity vectors through each passage, and the reference velocity is computed as the component of this velocity vector normal to the vertical section. The absolute geostrophic velocity is hence determined as the relative geostrophic velocity, referenced to the 1,000 dbar level, plus the reference velocity at this level, as obtained from float displacements.

The absolute geostrophic velocities allow computing the total geostrophic transports through each passage down to 2,000 m. These total transports are then decomposed into baroclinic and barotropic contributions, with the latter calculated as the fraction associated with the 2,000 m velocity and the former as the portion linked to the geostrophic velocity relative to this deep level. Further, the transports are computed for the entire water column down to the common deepest neutral density in all sections ($\gamma^n = 28.00$ kg m^{-3}) as well as for individual neutral-density layers, selected as to represent the different water masses in the region (Table 1; Arhan et al., 1999; Naveira Garabato et al., 2002; Reid et al., 1977; Sievers & Nowlin, 1984; Smith et al., 2010).

The location of several fronts is obtained from the maximum temperature gradients at 1,000 m (Figure 2). Once the fronts are located in all passages, we compute the water transports in those domains delimited by the fronts, both through the Drake and Northern Passages. For all our computations, we have used the frontal positions as obtained using the 2002–2018 average section, i.e., under the assumption that these positions are invariant. An analysis of its seasonal and interannual variability confirms that this is a reasonable assumption (Figure S1, Supporting Information).

The Argo floats drifting through the Scotia Sea can also be used to obtain the intra-annual (seasonal) and interannual variability of the density fields, reference velocities and transports. The amount of data (number of floats crossing and sampling the reference sections) changes throughout the year by as much as a factor of two (Table S1, Supporting Information), but it is sufficient for calculating seasonal changes from 3 months data sets, centered from January through December. For example, over these 3 months periods, the maximum number of float crossings the Drake Passage was 61 and the minimum was 29, while the maximum number of CTD casts within the 50 km wide strip was 66 and the minimum was 41. Considering that the Drake Passage section is about 860 km long, the latitudinal average resolutions (distance divided by number of floats) for calculating the reference velocities are between 16 and 30 km while, for building the hydrographic vertical sections, it is between 13 and 21 km.

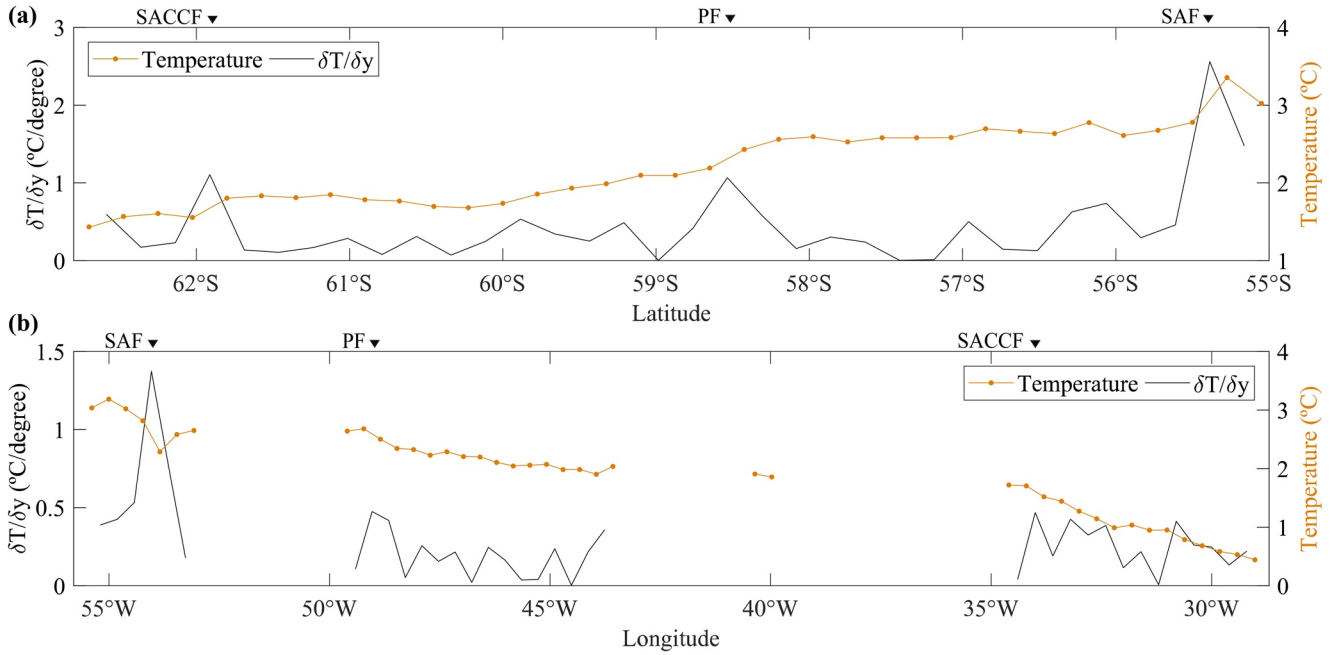

Figure 2. (a) Temperature (orange line) and temperature gradient (black line) at 1,000 m across the Drake Passage and (b) the North Scotia Ridge and Georgia Passages. The location of the Subantarctic Front (SAF), Polar Front (PF), and Southern Antarctic Circumpolar Current Front (SACCF) is shown.

In contrast, the distribution of data for different years is much less even. In order to avoid this intermittency, we have grouped the data in eleven 5 yr periods centered on every year between 2006 and 2016 (Table S2, Supporting Information). Because of the relatively small number of floats crossing the region during 2002 and 2003, we chose not to consider these two years (Table S3, Supporting Information). Over these 5 yr periods, the maximum and minimum number of floats crossing the Drake Passage was 112 and 65 while the maximum number of CTD casts within the 50 km wide strip was 95 and the minimum was 55. Considering the width of the Drake Passage, this provides reasonably good latitudinal average resolutions of 8–13 km for calculating the reference velocities and 9–15 km for building the hydrographic vertical sections over the 5 yr periods.

Finally, the procedure followed for each 3 months and 5 yr interval is the same as the procedure used for the entire data set. The seasonal variability is calculated as the standard deviation (SD) of the twelve 3 months calculations while the interannual variability is calculated as the SD of the eleven 5 yr realizations. Further, we use a simple procedure to assess the error bars associated with the reduction in the number of observations. The procedure consists of randomly reducing the casts and reference velocities in the 2002–2018 mean section to the actual number of casts and reference velocities for each one of the 3 months and 5 yr periods (Tables S1 and S2, Supporting Information); this is done 100 times for each case and the SD is calculated.

3. Results

3.1. Reference Velocities

All Argo floats analyzed in this study entered the Scotia Sea via the Drake Passage and drifted east and north. In Figure 3, we show the positions of all floats as they crossed the nominal location of the western and northern sections enclosing the Scotia Sea, and in Figure 4, we show the inferred 1,000 m velocity vectors.

The 1,000 m Argo float velocities are validated using two sets of ship acoustic Doppler current profiler (SADCP) velocities. The first one comes from the Drake Passage section between 64°W and 62°W (1979–2013) while the second one comes from the Laurence Gould Platform (2004–2018, with variable

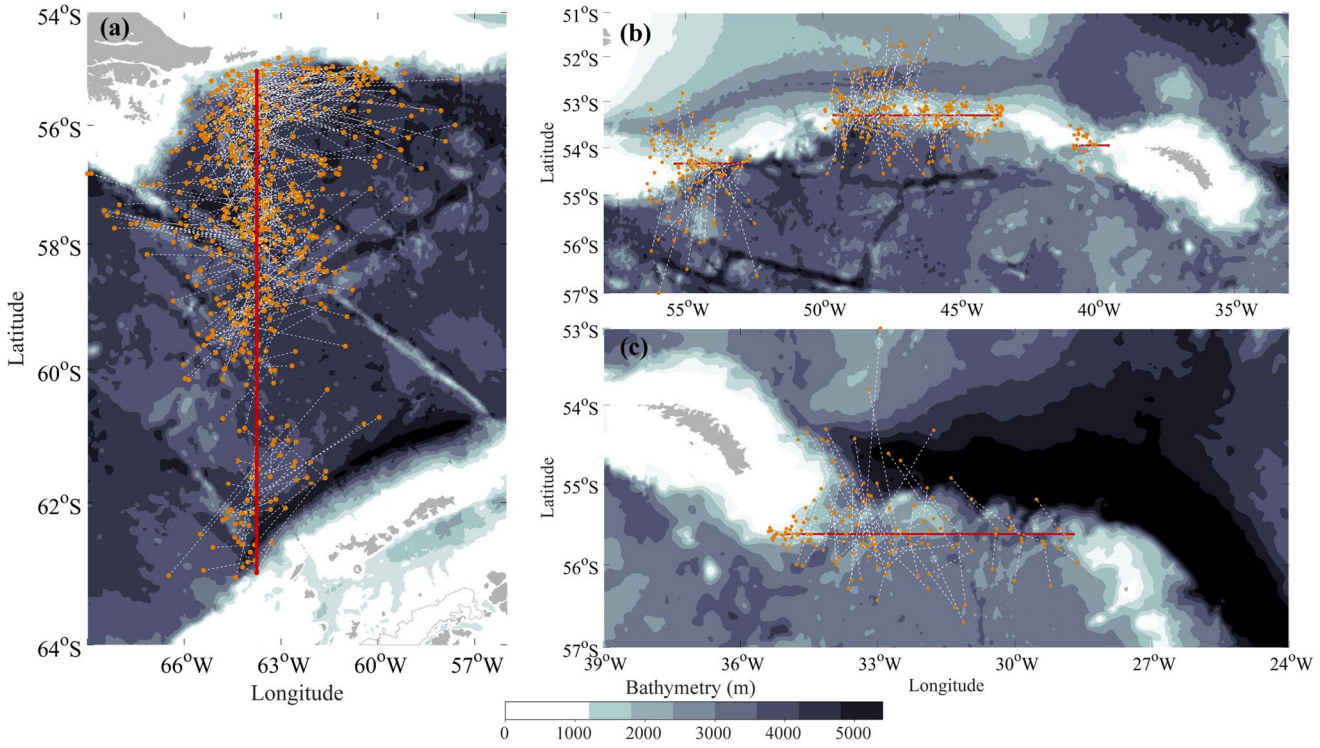

Figure 3. Argo floats crossing (a) the Drake Passage, (b) the North Scotia Ridge Passages (54–54, Shag Rocks and Black Rock), and (c) the Georgia Passage. A red line shows the location of the vertical sections across the passages. The orange dots show the surface float positions (last position before submerging and first position after surfacing), joined with a thin white dotted line. The white areas represent regions with water depth less than 1,000 m.

routes between the southern tip of South America and the Antarctic Peninsula), both included in the National Oceanic and Atmospheric Administration (NOAA) SADCP database (Caldwell et al., 2010). All data sets present velocities with similar patterns, with velocity maxima of 0.2–0.3 m s^{-1} between 55°S and 56°S (position of the SAF) and between 58°S and 59°S (PF location), and a more moderate increase (up to 0.1 m s^{-1}) near 62°S (SACCF position) (Figure 5). We have also estimated the errors in the 1,000 m reference velocities to be always well below 0.01 m s^{-1}, in good agreement with the velocity errors for these same passages according to the ANDRO database (Lebedev et al., 2007; Ollitrault & Rannou, 2013).

We count the number of floats that cross the Drake and Northern Passages considering only those floats launched relatively far from the passages section, specifically at least three profiling cycles away (30 days). The comparison of the normal-to-section velocities and the number of floats crossing 25 km long transects shows a high (and significant, $p < 0.01$) correlation between both variables: 0.85 for the Drake Passage and 0.75 for the Northern Passages (Figure 6). Both the peak zonal velocities and the largest number of floats entering the Scotia Sea correspond to the location of the SAF (55°S–56°S) and the PF (58°S–59°S), with fewer floats crossing east in between. South of 59°S, the number of floats is small yet non-negligible. In the northern boundary of the Scotia Sea, the largest velocities and highest number of floats are found in the 54–54 Passage (associated with the SAF), the Shag Rocks Passage (associated with the PF), and the Georgia Passage (associated with the SACCF). These significant correlations indicate that floats tend to get caught in the frontal jets, hence reducing the velocity uncertainties in those regions with the swiftest flow.

3.2. Vertical Sections

The Argo CTD casts, after gridding and low-pass filtering, can be used to represent the vertical distribution of temperature, salinity, neutral density, and normal-to-section geostrophic velocity (Figure 7). The sloping temperature, salinity, and density contours that characterize the SAF and PF show up clearly in the northern portion of the Drake Passage (Figure 7a). Relatively cold and salty waters are found at depth and south

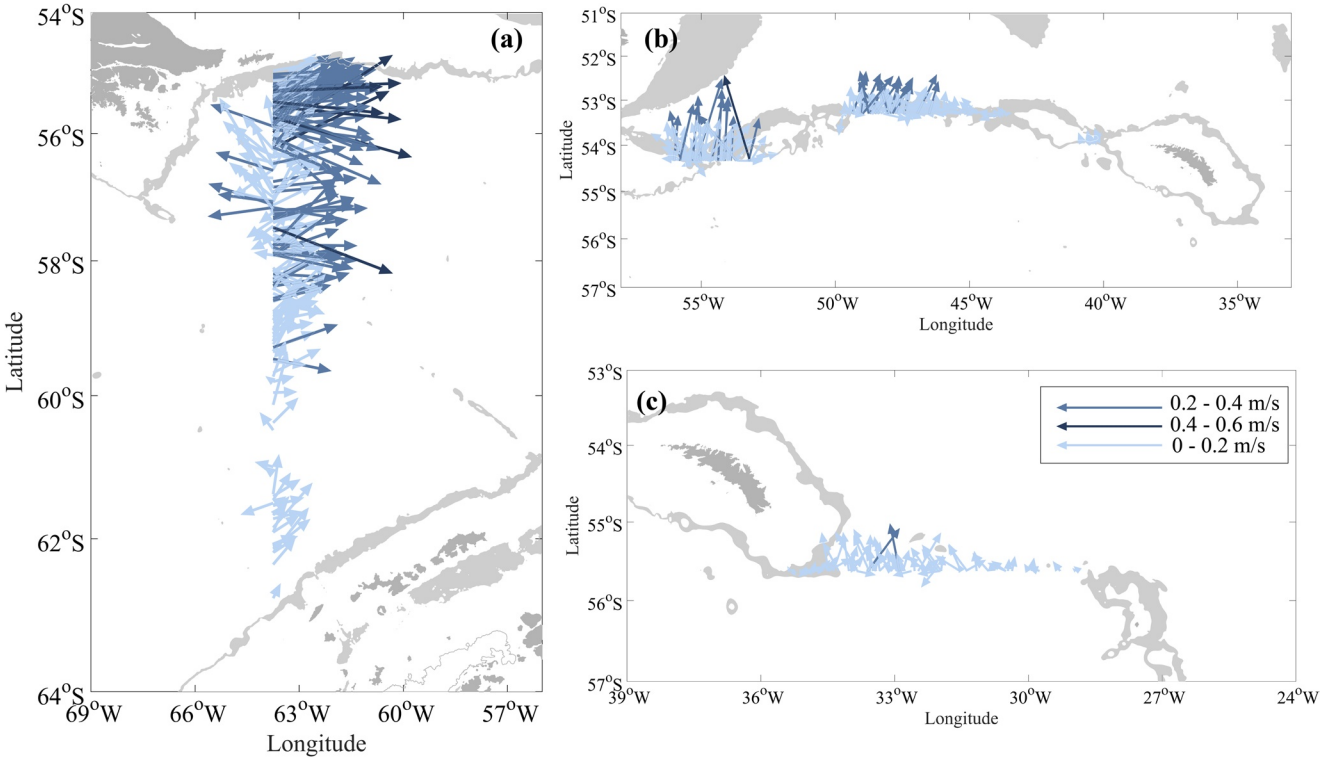

Figure 4. Velocity vectors at 1,000 m along the vertical sections in (a) the Drake Passage, (b) the North Scotia Ridge Passages (54–54, Shag Rocks and Black Rock), and (c) the Georgia Passage. The arrows denote the velocity vectors associated with all floats crossing the passages, colored according to their speed. The 1,000–2,000 m region is gray-shaded as to indicate the practical limits of our data.

of the PF (58°S–59°S). The temperature minima ($\theta < 0$°C) correspond to the near-surface southern waters (50–200 m), which are also relatively fresh, reflecting the relatively high precipitation (peak precipitation values in Antarctica, about 1,000–1,500 mm, take place in the western Antarctic Peninsula) and the summer melting of ice shelves and icebergs (Liu & Curry, 2010; Van Den Broeke & Van Lipzig, 2004). In contrast, the relatively warm surface waters in the South American side reveal the net annual-mean heat gain at these lower latitudes (Gille et al., 2016).

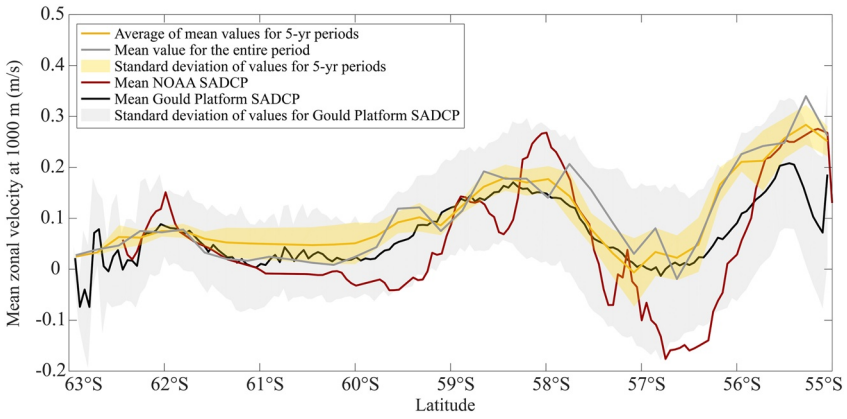

Figure 5. Mean 1,000 m zonal velocities cross the Drake Passage, as inferred from Argo floats (mean values for the entire period and average of the 5 yr period values), and as obtained with the NOAA SADCP data set and with the Laurence M. Gould platform. The shaded areas represent the standard deviations of values from the Laurence M. Gould data set.

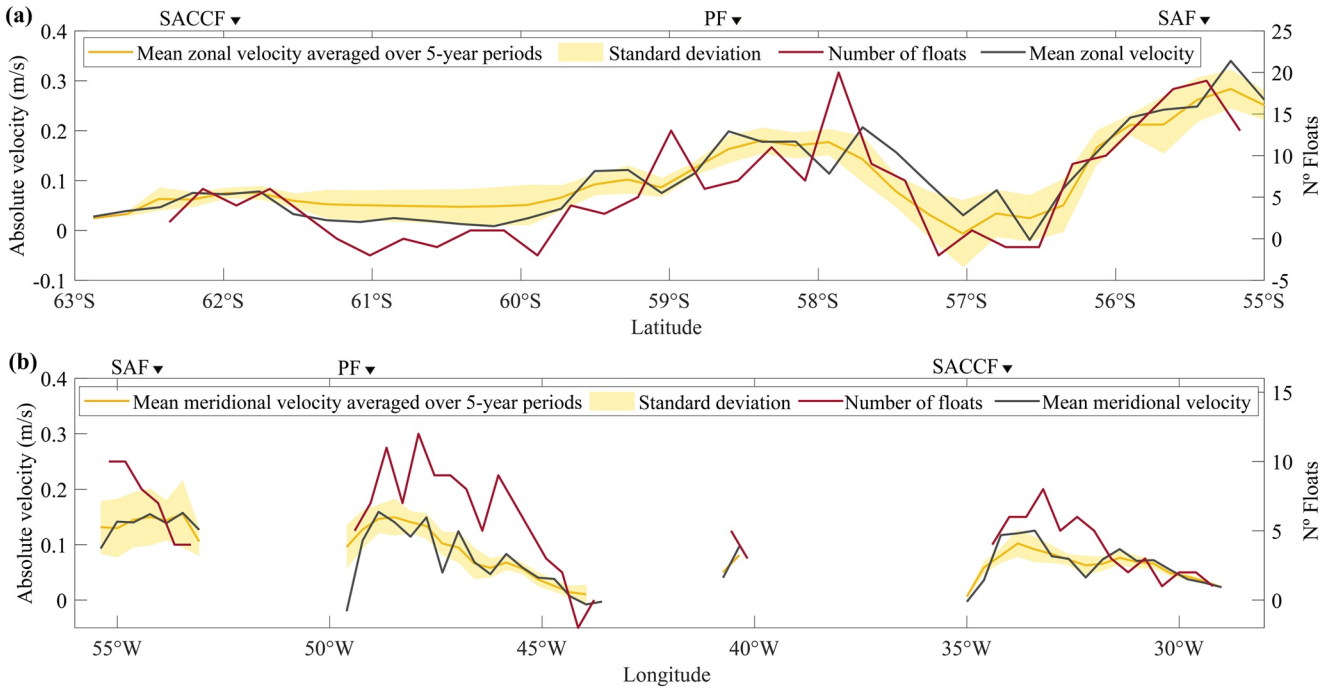

Figure 6. (Left axes) Normal-to-section 1,000 m velocities and (right axes) number of floats for the entire period (purple line) crossing 25 km long transects, for (a) the Drake Passage and (b) the Northern Passages. The velocities are calculated as the mean for the entire period (2002–2018; black line) and as the average of the 5 yr periods (2006–2016; orange line); in the last case the standard deviation is shown (yellow band).

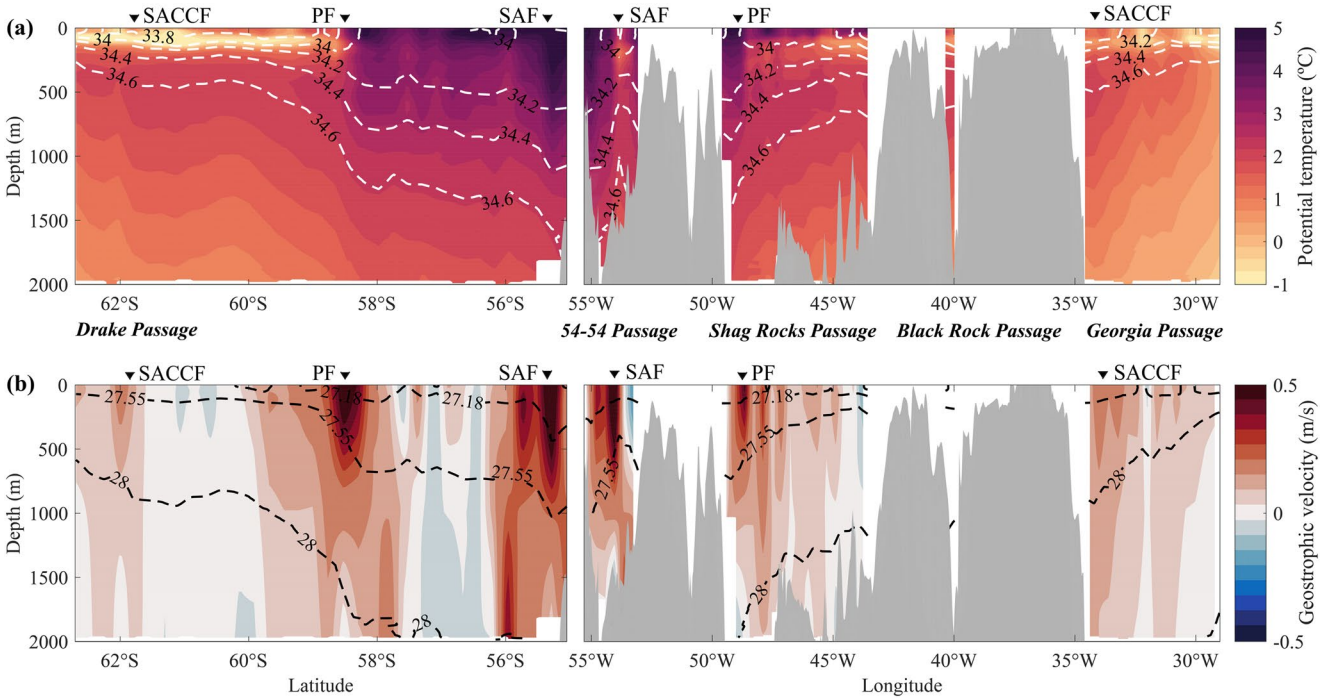

Figure 7. Vertical sections for (left) the Drake Passage and (right) the Northern Passages. (a) Potential temperature (colored, °C) and practical salinity (dashed contours). (b) Geostrophic velocity (colored, m s^{-1} in Drake Passage the positive values correspond to eastward velocities, for the Northern Passages the positive velocities correspond to northward velocities) and neutral density (dashed contours, kg m^{-3}; the selected isoneutrals denote the water mass boundaries in Table 1). The regional bathymetry is shaded in gray.

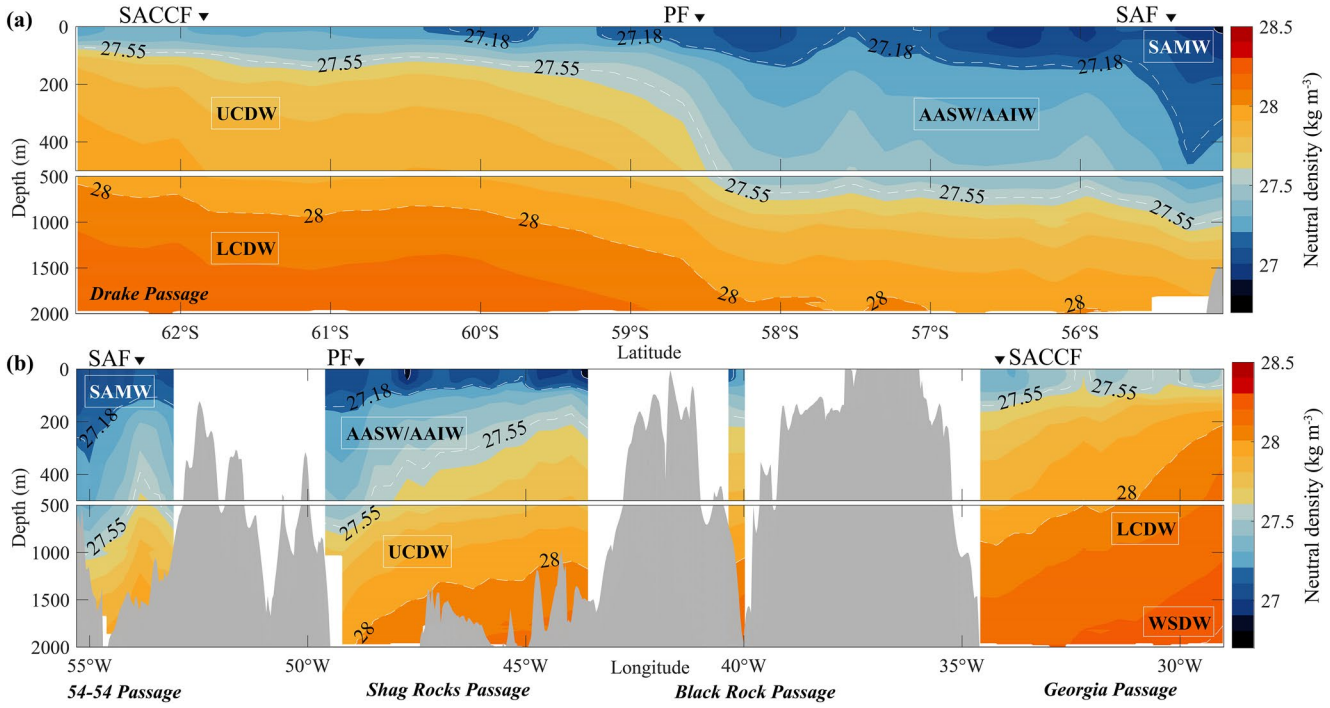

Figure 8. Density distribution across (a) the Drake Passage, and (b) the North Scotia Ridge (54–54, Shag Rocks and Black Rock) and Georgia Passages. The different water masses are labeled following the boundaries in Table 1.

The north-south temperature and salinity distribution in the Drake Passage are reflected by analogous west-east changes in the Northern Passages (Figure 7a). The SAF is located within the 54–54 Passage and the PF is found in the western portion of the Shag Rocks Passage. The Georgia Passage also reveals steep isolines, probably reflecting the presence of the two southernmost fronts (SACCF and SB). The relatively cold and fresh near-surface waters (50–200 m)–located south of the PF in the Drake Passage–are found east of the PF in the Northern Passages.

The density distributions confirm that the horizontal gradients in salinity and temperature drive a substantial density gradient, i.e., the thermohaline front turns into a density front (Figure 7b). This is true over most of the water column except in the near-surface region (50–200 m) south of the PF in the Drake Passage and east of the PF in the Northern Passages, where we find cold and fresh Antarctic surface waters. As a result, the density gradients are maximum at all depths in the SAF and deeper than 200 m in the PF.

The frontal systems show up clearly in the inferred velocity fields, with peak eastward velocities in excess or close to 0.5 m s^{-1} associated to the SAF (55°S–56°S in the Drake Passage and 54°W–55°W in the 54–54 Passage) and PF (58°S–59°S in the Drake Passage and 48°W–49°W in the Shag Rocks Passage) (Figure 7b). Further south in the Drake Passage (61.5°S–63°S) and east along the northern rim of the Scotia Sea (29°W–34°W in the Georgia Passage), we find the shallower and weaker currents associated with the southern SACCF; the SB is hardly seen as it appears very close to the continental shelf of the Antarctic Peninsula.

Some light SASW appears occasionally in Argo floats crossing the northern end of the Drake Passage and crossing the middle and eastern end of the Shag Rocks Passage, but its presence is ephemeral, and SASW barely shows up in the mean density sections (Figure 8). Further, only waters with neutral density less than 28.0 kg m^{-3} are fully sampled by the Argo floats (Figure 8). In the northern portion of the Drake Passage and the western part of the Shag Rocks Passage, the deepest waters have $\gamma^n = 28.0$ kg m^{-3} (in the 54–54 Passage, because of its relatively shallow bathymetry, the deepest waters do not even reach this value). In contrast, in most of the Drake and Northern Passages, at 2,000 m we find waters substantially denser than 28.0 kg m^{-3}. For this reason and under the assumption of zero diapycnal mixing, we will be able to close the water balances only down to $\gamma^n = 28.0$ kg m^{-3}, i.e., for the surface, mode, intermediate, and upper-circumpolar deep waters (Table 1).

Table 2
Total Geostrophic Transports Through the Passages Down to 2,000 m, With Their Baroclinic and Barotropic Contributions

	Passage	Total transport (Sv)	Baroclinic transport (Sv)	Barotropic transport (Sv)
Inflow	Drake	164.2 ± 10.8	55.6 ± 12.6	108.6 ± 12.8
Outflow	54-54	42.6 ± 5.6	15.5 ± 11.0	27.1 ± 11.3
	Shag Rocks	59.6 ± 7.2	32.1 ± 10.4	27.5 ± 13.2
	Black Rock	3.3 ± 1.5	2.9 ± 1.4	0.5 ± 0.7
	Georgia	53.8 ± 2.6	14.2 ± 1.4	39.6 ± 3.2
	Total Northern	159.3 ± 10.2	64.6 ± 19.6	94.7 ± 20.8

In the Drake Passage, the tilting isoneutrals are associated with the SAF near 55.5°S and with the PF near 58.5°S (Figure 8). In the northern half of the Drake Passage, the 28.0 kg m^{-3} isoneutral is fairly flat and close to 2,000 m while, from the PF southwards, this isoneutral progressively rises some 1,300 m, all the way to the Antarctica Peninsula. In the southern end of this section (near 62°S), because of the near-surface intrusion of relatively fresh waters, we observe the sloping isoneutrals mainly at depths greater than 200 m.

The latitudinal density distribution in the Drake transect is largely mirrored by the zonal distribution along the northern boundary of the Scotia Sea. The deepest western waters again have neutral densities close to γ^n = 28.0 kg m^{-3}. The SAF shows up in the middle of the 54–54 Passage and the PF is located in the western end of the Shag Rocks Passage. The 28.0 kg m^{-3} isoneutral and adjacent layers display large changes in depth in most of the Shag Rocks and Georgia Passages, in particular rising almost 700 m between the western and eastern ends of the Georgia Passage.

4. Discussion

4.1. Water Transports

The total water transports through the different passages down to 2,000 m are presented in Table 2. The total input through the Drake Passage is 164.2 ± 10.8 Sv, with a baroclinic contribution of 55.6 ± 12.6 Sv and a barotropic part of 108.6 ± 12.8 Sv. The total output through the Northern Passages is 159.3 ± 10.2 Sv, with baroclinic and barotropic shares of 64.6 ± 19.6 and 94.7 ± 20.8 Sv, respectively; overall, the outputs are roughly equally split among the 54–54, Shag Rocks and Georgia Passages (42.6, 59.6 and 53.8 Sv, respectively). This apparently suggests a fairly good water balance, with a net convergence of only 4.9 Sv into the Scotia Sea; however, this may be misleading, as the water layers are denser than γ^n > 28.0 kg m^{-3} are only partly represented in some of our vertical sections.

An alternative view would be to assess the water transports down to the 28.0 kg m^{-3} isoneutral, which are layers fully sampled in all sections enclosing the Scotia Sea. Down to this level, and under the assumption of along-isoneutral flow, we would expect that the water transport would be balanced. As expected, the absolute transports are lower: 140.8 ± 7.4 Sv entering through the Drake Passage (baroclinic and barotropic contributions of 42.8 ± 8.9 and 98.0 ± 7.4 Sv, respectively) and 115.9 ± 8.3 Sv exiting through the Northern Passages (baroclinic and barotropic parts of 45.8 ± 18.8 and 70.1 ± 19.3 Sv, respectively). The imbalance is now much larger than down to 2,000 m, with a total convergence of 24.9 Sv; most of this convergence corresponds to the AASW/AAIW (9.7 Sv) and UCDW (12.4 Sv) layers (Table 3). In the concluding section of this article, we will argue that this imbalance corresponds to water crossing the shallow regions in the Northern Passages.

The spatial distribution of water transports per layer is summarized in Figure 9. The zonal transports through the Drake Passage are clustered around the frontal systems: SAF (55°S–56°S), PF (58°S–59°S), and

Table 3
Total Geostrophic Transports per Layer Through the Passages Down to γ^n = 28.0 kg m^{-3}

Layer (γ^n, kg m^{-3})	Drake (Sv)	Northern (Sv)	54–54 (Sv)	Shag Rocks (Sv)	Black Rock (Sv)	Georgia (Sv)
SAMW (26.90–27.18)	12.8	10.0	5.3	4.7	-	-
AASW/AAIW (27.18–27.55)	44.0	34.3	15.0	15.7	0.4	3.2
UCDW (27.55–28.00)	84.0	71.6	20.6	31.2	2.0	17.8
All (<28.00)	140.8	115.9	40.9	51.6	2.4	21.0
Barotropic (<28.00)	98.0	70.1	24.2	25.4	2.0	18.5
Baroclinic (<28.00)	42.8	45.8	16.7	26.1	0.4	2.5

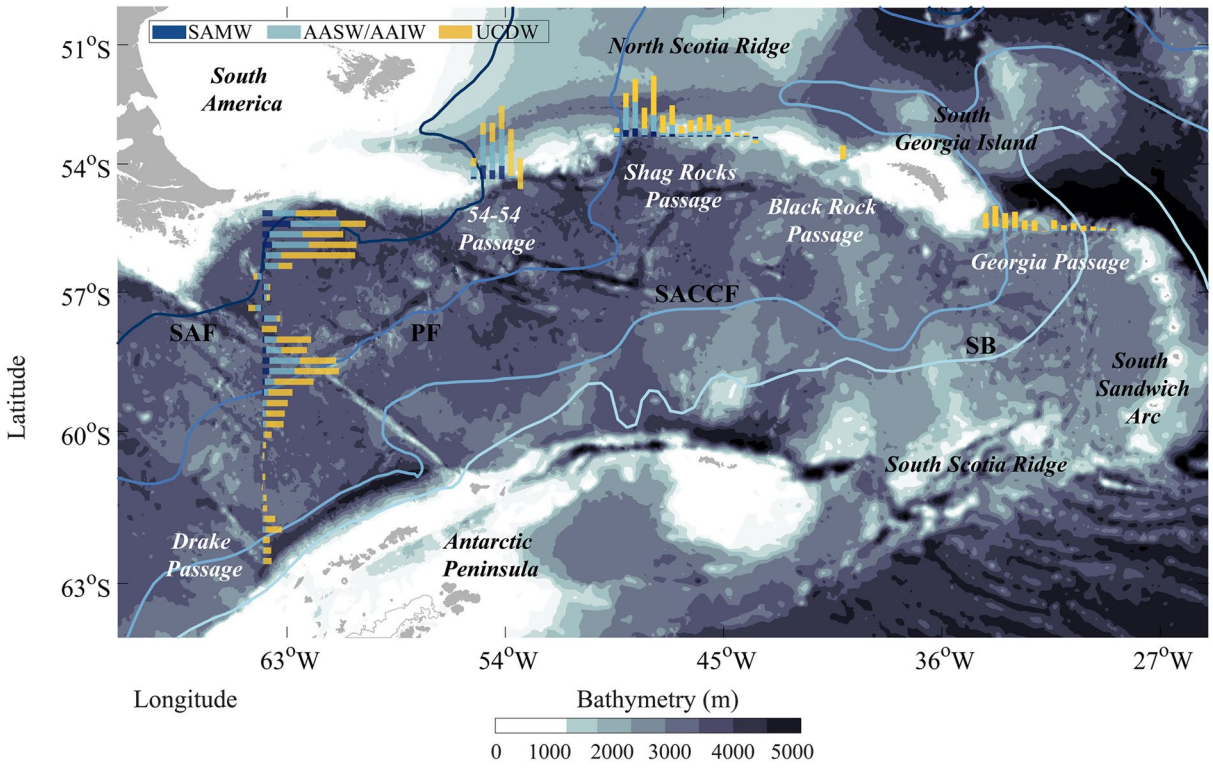

Figure 9. Transports per water mass (down to $\gamma^n = 28.0$ kg m^{-3} at 25 km intervals) crossing each passage. The color bars illustrate the partitioning of the transports among different water masses (dark blue, SAMW; light blue, AASW/AAIW; yellow, UCDW). The surface location of the different fronts comes from Greene (2020) through Orsi and Whitworth (2005), using all historical hydrographic data available for the Southern Ocean and frontal definitions from Orsi et al. (1995).

SACCF (52°S–63°S). Similarly, the meridional transports through the Northern Passages are also dominated by the along frontal flow: SAF (54°W–55°W), PF (48°W–49°W), and SACCF (33°W–34°W).

The relative contribution of mode and intermediate waters vs. UCDW changes in a similar fashion both latitudinally and zonally: the largest contribution of the mode and intermediate waters is in the northern half of the Drake Passage and in the 54–54 and Shag Rocks Passages, while the largest fraction of UCDW is in the southern half of the Drake Passage and in the Georgia Passage (Figure 9). In particular, the SAMW outflow occurs entirely through the North Scotia Ridge discontinuities and is totally absent in the Georgia Passage; in contrast, we find AASW/AAIW, UCDW, and LCDW in all passages. A small presence of WSDW in the eastern part of the Georgia Passage is also visible in the water transports down to 2,000 m (Figure S2, Supporting Information).

4.2. Cross-Frontal Exchange

Frontal systems are often thought to act as barriers to different water masses but they are also the source of mesoscale and submesoscale instabilities that induce cross-frontal transfer. With this idea in mind, we wish to track the amount of water that enters through the Drake Passage between the frontal systems (as defined in Section 2.3) and how these waters are distributed between these same fronts when crossing the Northern Passages.

The three main frontal systems in the Drake Passage (from north to south: SAF, PF, and SACCF) are also traceable in the Northern Passages: SAF reaches the 54–54 Passage, PF the Shag Rocks Passage, and SACCF the Georgia Passage (Figures 2, 7, and 8). Therefore, we are interested in exploring not only how the water entering through the Drake Passage exits through the Northern Passages (Tables 3 and 4) but also to assess if there is some conservancy of the transports between the frontal systems that reflects some dynamical pathways. The results suggest that there are substantial mass transformations, with the region between

Table 4
Geostrophic Transports Between Fronts and Through the Different Passages Down to $\gamma^n = 28.0$ kg m^{-3}: Inflow Through Drake Passage and Outflow Through the Northern Passages

Drake	**S.A.-SAF**		**SAF-PF**			**PF-SACCF**	**SACCF-A.P.**
	18.1		83.2			34.4	5.1
Northern	**S.A.-SAF**	**SAF-53°W**	**49°W-PF**	**PF-47°W**	**41°W-40°W**	**34°W-33°W**	**33°W-29°W**
	25.0	15.9	4.5	47.1	2.4	4.5	16.5
	25.0		20.4		54.0		16.5
	54-54		**Shag Rocks**		**Black Rock**	**Georgia**	
	40.9		51.6		2.4	21.0	

Note. The longitudes roughly indicate the geographical boundaries (Figure 9).
Abbreviations: S.A. stands for South America, A.P. stands for Antarctic Peninsula, and S.S.A. stands for the South Sandwich Arc.

the SAF and the PF losing as much as 62.8 Sv while all other regions gain water transport; north-west of the SAF gains 6.9 Sv, the region between PF and SACCF gains 19.6 Sv, and south-east of the SACCF gains 11.4 Sv (Table 5).

A complementary view of how water transport remains both blocked and mixed by the frontal systems is provided by the floats' trajectories. These trajectories will resemble mostly the motions at the 1,000 m parking depth, modified by the relatively short period when the floats do their vertical cycle and remain at the sea surface. Nevertheless, because of the predominance of the barotropic contribution and since the geostrophic contribution is aligned with the frontal systems, we expect that the flow direction at all depths will remain similar to the 1,000 m flow heading (Figure 7b).

The principal pathways for those floats crossing the Drake Passage on either side of a front (Section 2.3) are shown in Figure 10. The results are consistent with the transports between fronts as reported in Table 5, with those floats entering between the SAF and the PF (Figure 10b) being most dispersed; only 29% of the floats remain between these fronts, with the losses split fairly equally between the adjacent domains. The floats north of the SAF and south of the SACCF also display substantial scattering. In contrast, those floats crossing the Drake Passage between the PF and the SACCF appear to experience the fewest losses (Table 5).

Table 5
Number of Argo Floats Entering and Departing the Scotia Sea Between Frontal Systems; Only Those Floats That Exit the Scotia Sea are Considered

		Output			
		S.A.-SAF	SAF-PF	PF-SACCF	SACCF-A.P.
Input		53	46	70	18
S.A.-SAF	22	11	7	4	0
SAF-PF	119	40	34	37	8
PF-SACCF	40	2	5	25	8
SACCF-A.P.	6	0	0	4	2

Note. The numbers in the first column indicate the floats entering through the Drake Passage and the numbers in the top row represent the floats exiting through the Northern Passages; the figures in each cell represent the number of floats entering and leaving through the corresponding frontal domain.
Abbreviations: S.A. stands for South America, A.P. stands for Antarctic Peninsula, and S.S.A. stands for the South Sandwich Arc.

Finally, we can use the time taken by floats to cross from the Drake to the Northern sections to estimate the mean residence time of water masses near 1,000 m in the Scotia Sea. The residence time for individual floats changes greatly, from as little as 20 days for those floats entering through the northern edge of the Drake Passage to as much as three years for those crossing through the southern end (Figure 11). Considering only those floats that cross the Scotia Sea, the mean residence time is 219 ± 213 days. According to the location of these floats, as they cross the Drake Passage, the mean residence is 45 ± 30 days for those floats entering between S.A. and the SAF, 223 ± 213 days for floats entering between SAF and PF, 266 ± 226 days for those entering between PF and SACCF, and 443 ± 77 days for those crossing the Drake Passage between SACCF and S.S.A. The Scotia Sea has an area of about 900,000 km^2, and the corresponding volume down to 2,000 m is about 1.8×10^{15} m^3; therefore, a residence time of 219 days (7.3 months) would represent an average water transport of 95 Sv, which is not too far from our 2,000 m barotropic transport through the Drake Passage (109 Sv).

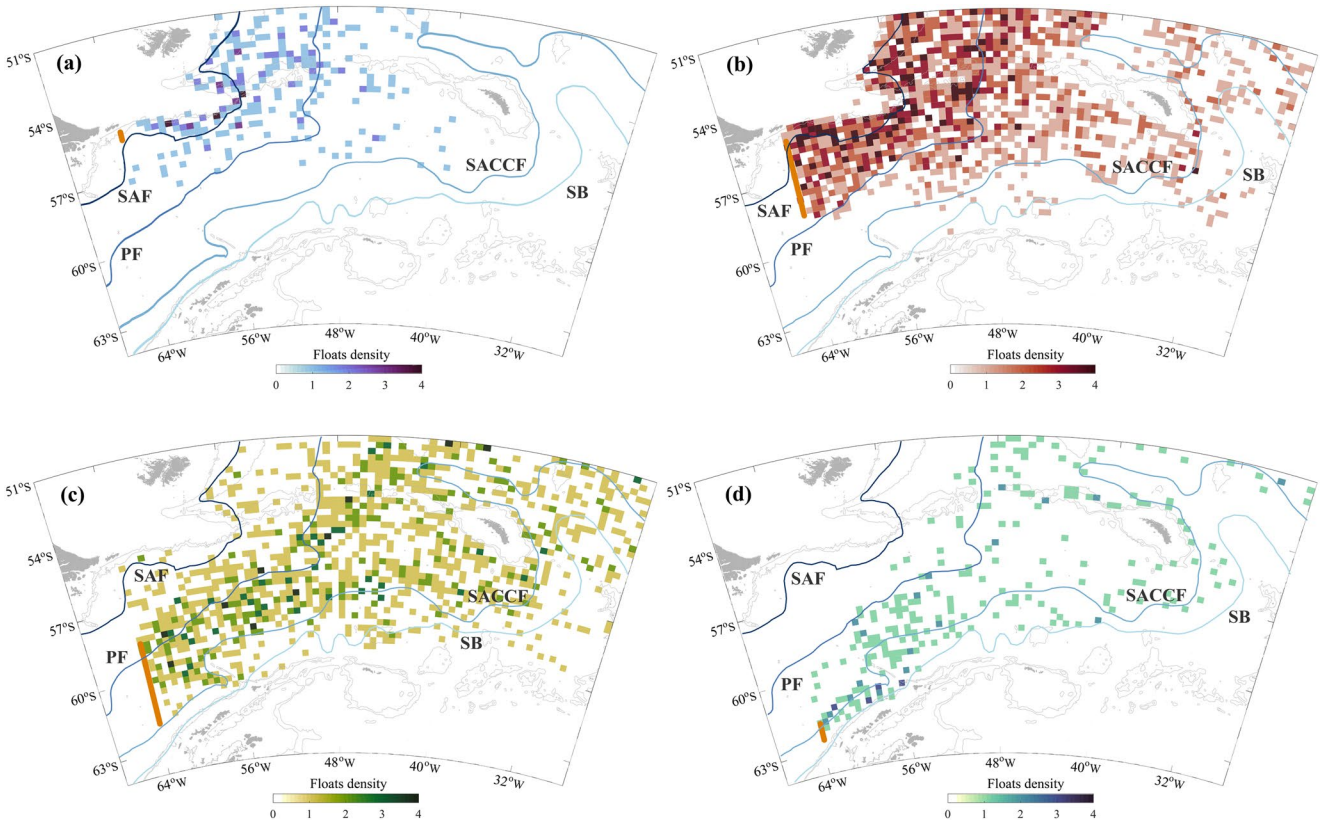

Figure 10. Number of floats that drift in the Scotia Sea after entering through the Drake Passage, counted over 0.25° × 0.5° latitude-longitude grid elements. The floats are identified and counted by their latitude of origin, represented by orange lines, in Drake Passage: (a) South America to SAF, (b) SAF to PF, (c) PF to SACCF, and (d) SACCF to the Antarctica Peninsula. The surface location of the different fronts, as defined by Orsi et al. (1995), comes from Orsi and Whitworth (2005) and available in the Greene (2020) data set.

4.3. Interannual Variability

Intense atmospheric forcing can modify the slope of isopycnals across the Southern Ocean and therefore influence the baroclinic transport of the ACC (Kim & Orsi, 2014; Rintoul & Naveira Garabato, 2013; Sokolov and Rintoul, 2009a, 2009b). Hence, we split the Argo data into 5 yr overlapping periods in order to calculate the interannual variability. The mean density and normal-to-section velocity fields can be calculated by averaging the 5 yr period data, providing a total of 11 realizations centered from 2006 to 2016 (utilizing data spanning the 2004–2018 period). The resulting mean fields are nearly indistinguishable from the mean fields obtained using the full set of floats (Figures 7 and 8, and Figure S3, Supporting Information).

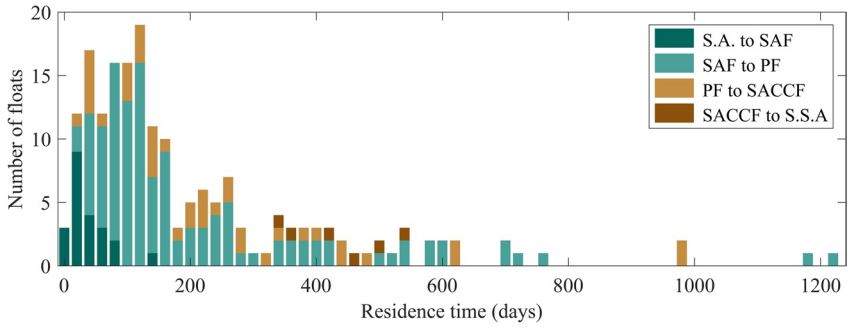

Figure 11. Number of floats as a function of residence time in the Scotia Sea, split according to their position between frontal systems as they enter the Drake Passage: South America (S.A.) to SAF, SAF to PF, PF to SACCF, and SACCF to the South Sandwich Arc (S.S.A.). Each bar width corresponds to 20 days of residence time.

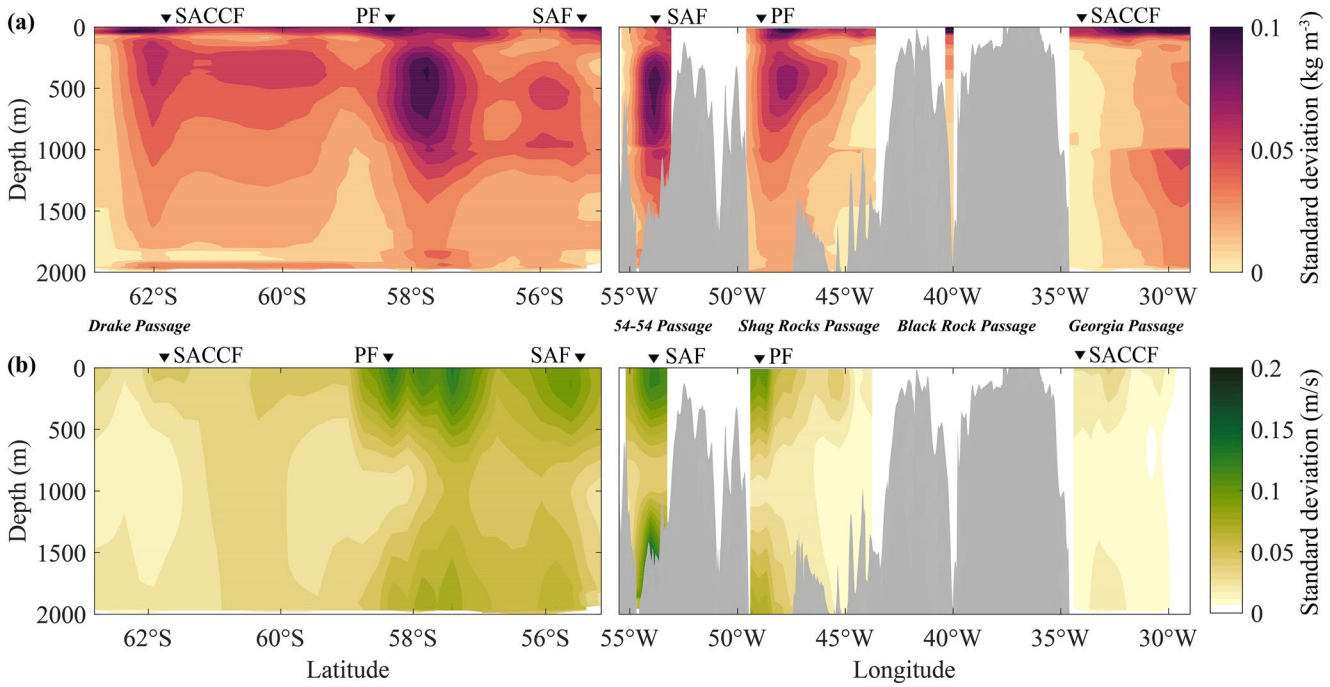

Figure 12. Standard deviation of the 5 yr averaged fields of (a) density and (b) geostrophic velocity for (left panels) the Drake Passage and (right panels) the Northern Passages (Black Rock passage has been omitted in the geostrophic velocity).

Additionally, the changes in the latitudinal and longitudinal positions of the 1,000 m fronts are relatively small and are therefore ignored (Figure S1, Supporting Information).

The variability in the density and velocity fields is calculated as the SD of these 11 realizations (Figure 12). The SD in the density fields is largest in the surface waters and in the frontal regions, particularly in the PF for the Drake Passage and the SAF for the Shag Rocks Passage (Figure 12a). The SD in the 1,000 m reference velocity is fairly constant everywhere, about 0.05 m s^{-1} (Figure 5). The SD in the geostrophic velocity fields is somewhat large in the upper 500 m of the SAF and PF regions (peak values up to 0.15 m s^{-1}) both in the Drake and Northern Passages (Figure 12b); in particular, there is high latitudinal variability associated with the PF in the Drake Passage.

The water transports through the Drake and Northern Passages, split among all three water masses, are shown in Figure 13; the Black Rock Passage is omitted because there are too few floats to calculate a trend. The error bars represent our best estimate of the variability associated with the reduction in the number of float casts and tracks for each 5 yr period, as explained in Section 2.3.

The transports through the Drake, Shag Rocks, and Georgia Passages are fairly stable. The input through the Drake Passage ranges between 145.3 and 166.5 Sv, though the differences are not significant. The outflow through the Shag Rocks Passage is also fairly constant, always in the 55–60 Sv range except for a decrease between 2010 and 2012, which reaches as low as 44.9 Sv. In contrast, there is a negative overall trend in the output through the 54–54 Passage, from 52.8 down to 35.6 Sv, which shows steady between 2013 and 2016. Additionally, during these last years (2011–2016) the transport through the Georgia Passage increases between 17.3 and 21.9 Sv, although the variation is barely significant.

The transport variations in these passages may be attributable to differences in both the AASW/AAIW and UCDW masses. In particular, the decrease in transport through the 54–54 Passage is caused by a substantial decrease in both AASW/AAIW and UCDWs, while the increase in transport through Georgia Passage during the last years appears mostly associated with an increase in UCDW. A transfer of outflow waters from intermediate-west (54–54 Passage) to deep-east (Georgia Passage) appears plausible during the last 5 yr periods.

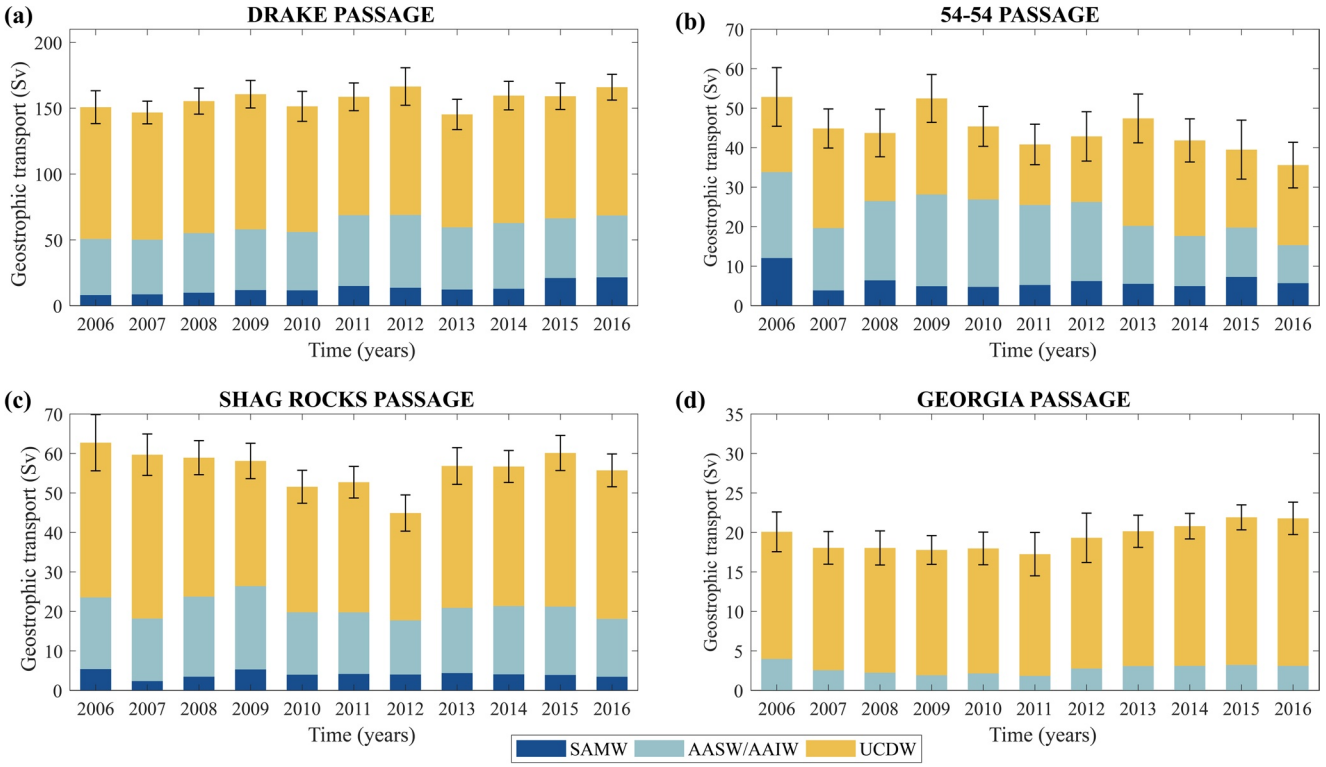

Figure 13. Total geostrophic transports through the passages down to $\gamma^n = 28.0$ kg m^{-3}, averaged over 5 yr periods, between 2006 and 2016: (a) Drake Passage, (b) 54–54 Passage, (c) Shag Rocks Passage, and (d) Georgia Passage. The contribution of each water mass and the error bars in the total transports are shown. Notice the change in the vertical scale from one panel to another.

4.4. Seasonal Variability

We also split the Argo data in 3 months intervals in order to obtain the seasonal variability. The mean density and normal-to-section velocity fields, per month, can be calculated by a running 3 months average of the data. The resulting mean fields are analogous to the mean fields obtained using the full set of floats (Figures 7 and 8, and Figure S4, Supporting Information). As for the 5 yr case, the latitudinal and longitudinal positions of the fronts are fairly stable and variations are therefore ignored (Figure S1, Supporting Information).

The variability in the density and velocity fields is calculated as the SD of the twelve 3 months realizations. The SD in the density fields is analogous to the interannual values, yet smaller below 1,000 m and larger in the seasonal mixed layer (Figure 14a); this high surface variability reaches deeper (as much as 100 m) between the PF and the SAF. The SD in the 1,000 m reference velocity is fairly small, with peak values less than 0.08 m s^{-1} in the frontal regions. The SD in the geostrophic reference velocity again resembles the interannual fields, with maxima at the surface (Figure 14b). In the Drake Passage, the seasonal SD values are smaller than the interannual ones; further, the peak values stretch all the way between the two fronts rather than being located at the fronts themselves. In the Northern Passages, the peak SDs are associated with the SAF in the 54–54 Passage.

The seasonal variability of the water transports through the Drake and Northern Passages is substantial (Figure 15; again, the Black Rock Passage is omitted). The error bars show the potential effects of the reduced number of float casts and tracks for each realization, as explained in Section 2.3.

The water input through the Drake Passage ranges between 110.8 and 174.1 Sv, with a minimum in autumn and winter (March through June; we always refer to austral seasons). The seasonal change is mainly caused by fluctuations in both the AASW/AAIW and UCDW transports.

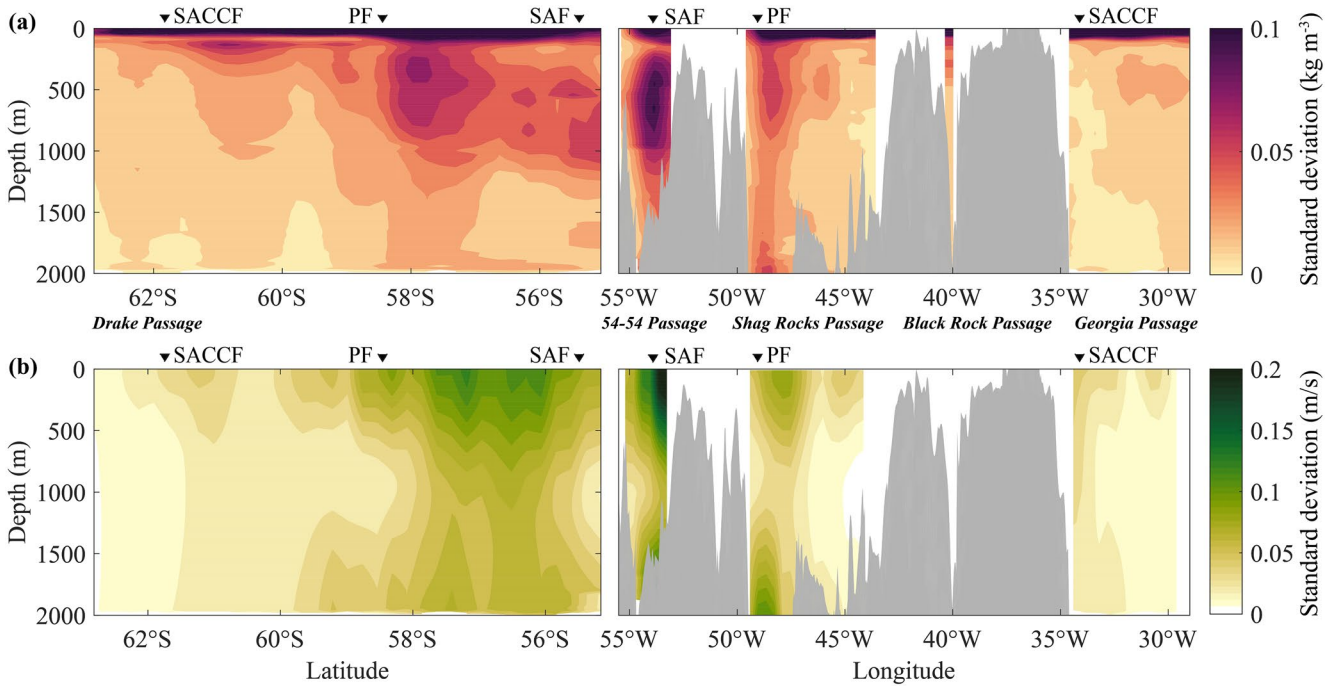

Figure 14. Standard deviation of the 3 months averaged fields. (a) Density and (b) geostrophic velocity for (left panels) the Drake Passage and (right panels) the Northern Passages (Black Rock passage has been omitted in the geostrophic velocity).

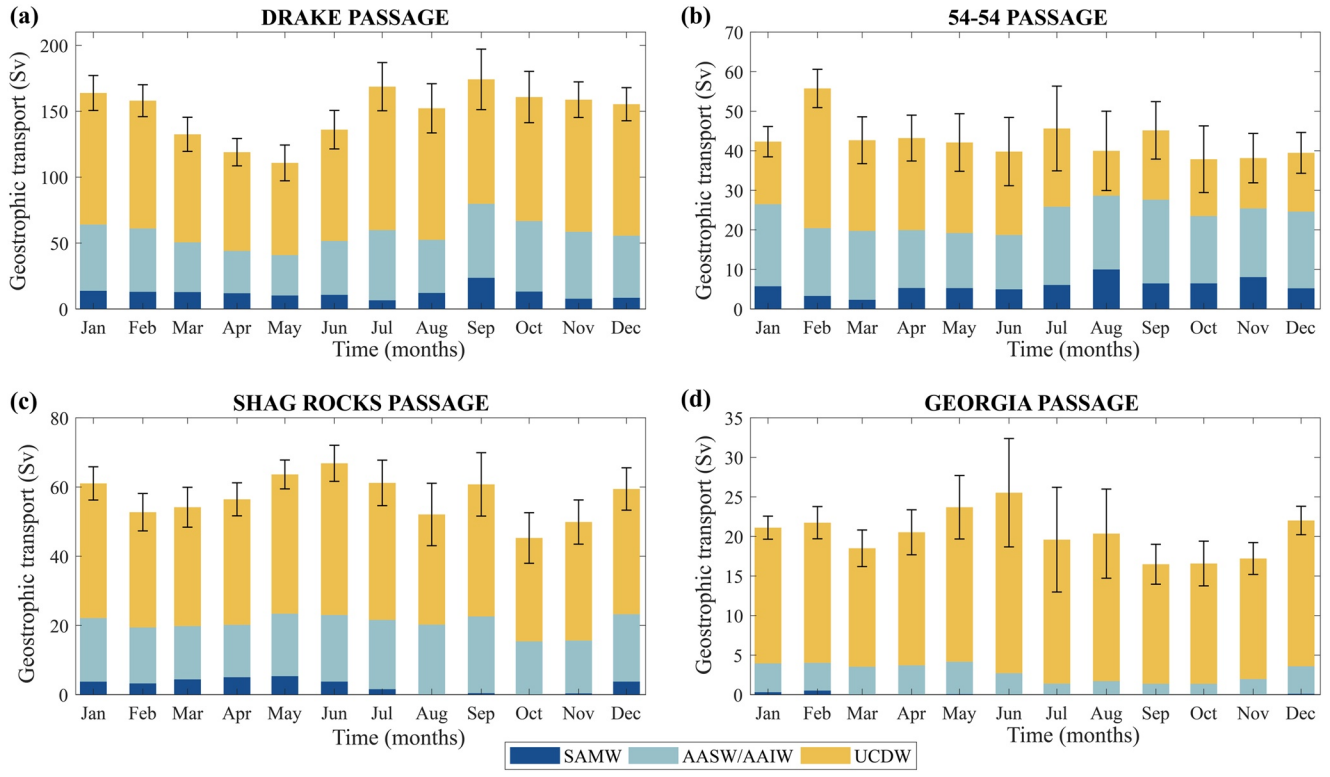

Figure 15. Total geostrophic transports through the passages down to $\gamma^n = 28.0$ kg m^{-3}, averaged over 3 months intervals: (a) Drake Passage, (b) 54–54 Passage, (c) Shag Rocks Passage, and (d) Georgia Passage. The contribution of each water mass and the error bars in the total transports are shown. Notice the change in the vertical scale from one panel to another.

Table 6
Comparison of Barotropic, Baroclinic and Total Transports (Sv) Through the Different Passages According to Several Authors and This Study

	Drake (Sv)			North Scotia Ridge (Sv)			Georgia (Sv)		
Author	Barotropic	Baroclinic	Total	Barotropic	Baroclinic	Total	Barotropic	Baroclinic	Total
Whitworth et al. (1982)	-	-	117 to 144	-	-	-	-	-	-
Whitworth and Peterson (1985)	-	-	134 ± 11	-	-	-	-	-	-
Whitworth and Peterson (1985) (2,500 m)	-	-	125 ± 13	-	-	-	-	-	-
Ganachaud and Wunsch (2000)	-	-	140 ± 6	-	-	-	-	-	-
Sloyan and Rintoul (2001)	-	-	135 ± 1	-	-	-	-	-	-
Thorpe et al. (2002)	-	-	-	-	-	-	-	14.5 ± 1.5	-
Meredith et al. (2003)	-	-	-	-	-	-	4.3	9.8	14.1
Cunningham et al. (2003) (3,000 m)	-	107 ± 10	-	-	-	-	-	-	-
Cunningham et al. (2003)	-	-	137 ± 8	-	-	-	-	-	-
Gille (2003)	23 ± 2	98 ± 5	121 ± 6						
Naveira Garabato et al. (2003)	-	-	143 ± 13		-	119 ± 12	-	-	30 ± 10
Firing et al. (2011) (1,000 m)	-	-	95 ± 2	-	-	-	-	-	-
Firing et al. (2011)	-	-	154 ± 38						
Koenig et al. (2014) (3,000 m)	5 ± 16	136 ± 11	141 ± 13	-	-	-	-	-	-
Chidichimo et al. (2014) and Donohue et al. (2016)	46 ± 9	128 ± 6	173 ± 11	-	-	-	-	-	-
Colin de Verdière and Ollitrault (2016)	-	-	175	-	-	-	-	-	-
Smith et al. (2010)	-	-	-	73	44	117 ± 10	-	-	-
This study (2,000 m)	108.6 ± 12.8	55.6 ± 12.6	164.2 ± 10.8	55.1 ± 19.9	50.4 ± 19.1	105.5 ± 10.4	39.6 ± 3.2	14.2 ± 1.4	53.8 ± 2.6
This study (28.0 kg m^{-3})	98.0 ± 7.4	42.8 ± 8.9	140.8 ± 7.4	51.4 ± 18.6	43.5 ± 18.9	94.9 ± 8.1	18.5 ± 1.3	2.5 ± 0.5	21.0 ± 1.7

Note. The velocity reference level is indicated between parenthesis in the first column. For this study, the SD corresponds to the value obtained from the 5-year values between 2006 and 2016 (Table 3 shows, for this study, how the output splits among the 54–54, Shag Rocks and Black Rock Passages).

The transport in the Shag Rocks Passage is minimum in spring and maximum in winter (45.3–66.8 Sv range) while in the 54–54 Passage the transport is more stable, with a minimum in early summer (37.8 Sv). Finally, in the Georgia Passage again the minimum transport occurs in spring and the maximum in summer (16.5–25.6 Sv range). These seasonal variations are associated with changes in all water masses, with the winter disappearance of SAMW in Shag Rocks Passage and AASW/AAIW in Georgia Passage.

4.5. Comparison With Previous Estimates

Previous estimates of water transport through the Drake Passage range between 121 and 173 Sv (Table 6). When referenced to a deep-water level, these estimates remain very large: 125 Sv (referenced to 2,500 m, Whitworth & Peterson, 1985) and 141 Sv (referenced to 3,000 m, Koenig et al., 2014). Using deep or near-bottom velocities, the barotropic contribution is relatively small (ranging between 5 and 41 Sv) as compared with the baroclinic one (from 98 to 136 Sv) (Chidichimo et al., 2014; Donohue et al., 2016; Gille, 2003; Koenig et al., 2014). In contrast, there are only a few previous estimates of water transport through the North Scotia Ridge and Georgia Passages (Table 6). Naveira Garabato et al. (2003) estimated the output through these Northern Passages to be 119 and 30 Sv, respectively; this total output, 149 Sv, is only slightly above their estimate for the water input through the Drake Passage (143 Sv). More recently, Smith et al. (2010) have estimated that 117 Sv exit through the North Scotia Ridge Passages.

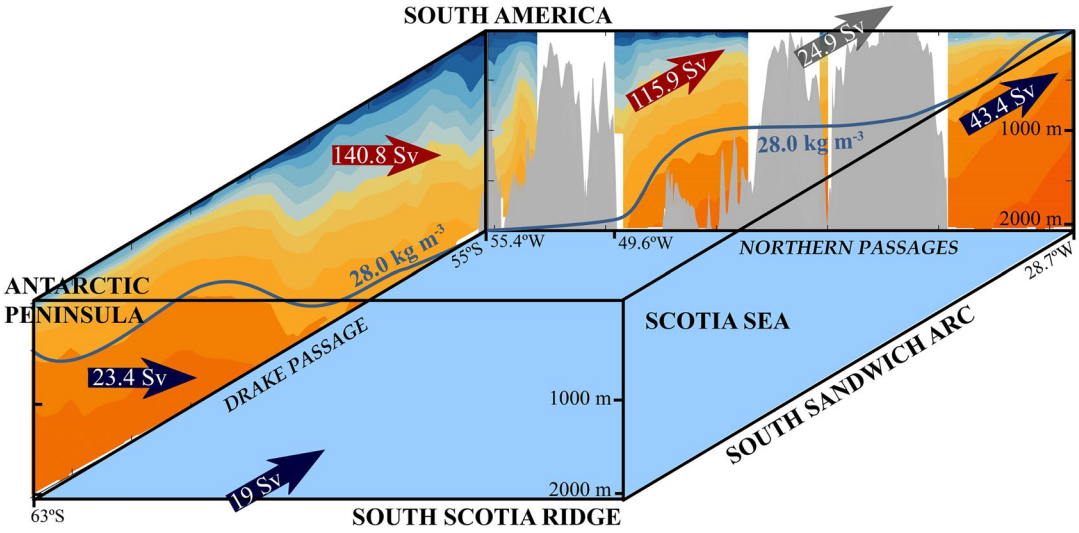

Figure 16. Schematics of input and output transports in the Scotia Sea. The solid arrows represent the calculated transports, and the dashed arrows represent the transports through the shallow Northern Passages.

Our results for the water transport through the Drake Passage are 164.2 ± 10.8 Sv for the water column above 2,000 m and 140.8 ± 7.4 Sv for waters shallower than the 28.0 kg m^{-3} isoneutral surface (Table 6). We have also found that the transports through the Northern Passages are 159.3 ± 10.2 Sv down to 2,000 m and 115.9 ± 8.3 Sv down to the 28.0 kg m^{-3} isoneutral. The mean transports through the Northern Passages down to the 28.0 kg m^{-3} isoneutral surface are split into 40.9, 51.6, 2.4, and 21.0 Sv for the 54–54, Shag Rocks, Black Rock, and Georgia passages, respectively. The 43.4 Sv that inflow through the Drake Passage between the 28.0 kg m^{-3} isoneutral and the 2,000 m level outflows the Scotia Sea mostly through the Georgia Passage (32.8 Sv).

Our mean-transport estimates through the Drake Passage (140.8 Sv down to 28.0 kg m^{-3} and 164.2 Sv down to 2,000 m) are in the high range of previous estimates. We may indirectly assess the robustness of these results by comparing these inputs with the outputs through the Northern Passages. Considering layers lighter than 28.0 kg m^{-3}, about two-thirds of the input and output transports correspond to UCDW and one-third to the intermediate layers (AASW/AAIW), with the SAMW representing only about 5%–10% of the total. Down to 2,000 m, the input-output imbalance is small (input exceeds output by 4.7 Sv), although these numbers do not consider the water inflow through the South Scotia Ridge. In contrast, the imbalance increases to 24.9 Sv for isoneutrals lighter than 28.0 kg m^{-3}.

Previous studies indicate that there are 19 ± 7 Sv of LCDW and WSDW entering the Scotia Sea through the South Scotia Ridge (Naveira Garabato et al., 2003; Thorpe et al., 2002). Adding this transport to the 23.4 Sv that inflow through the Drake Passage between 28.0 kg m^{-3} and 2,000 m, gives a total of 42.4 Sv, which fits very well the outflow of 43.4 Sv through the Northern Passages between 28.0 kg m^{-3} and 2,000 m. Hence, we are left with about 25 Sv of unaccounted outflow through the northern and eastern Passages down to 28.0 kg m^{-3} (Figure 16). We propose that these 25 Sv will flow out through areas of the North Scotia Ridge Passages that are unsampled by the Argo floats; considering that these shallow cross-sections have an area of about 250 × 10^6 m^2 (Figure 8), this outflow would be accounted by a mean velocity of about 0.1 m s^{-1}.

The Argo data set does not allow computing the water transports below 2,000 m. If we compare our Drake Passage transports down to 2,000 m, 164.2 ± 10.8 Sv, with the upper range of all previously reported values, 173–175 Sv (Chidichimo et al., 2014; Colin de Verdière & Ollitrault, 2016; Donohue et al., 2016), about 10 Sv would enter the Scotia Sea through the lower part of the water column. Considering the relatively shallow depths of the Northern Passages, this additional input could find its way out of the Scotia Sea more easily through the deepest point of the Shag Rocks Passage (Smith et al., 2010) or veering eastward through the Georgia Passage.

Figure 17. Water transports through the Drake (blue line) and Northern (red line) Passages, from the sea surface down to the 28.0 kg m^{-3} isoneutral. (a) Seasonal and (b) interannual variations; the SDs of the time series are represented as shaded colored bands.

5. Concluding Remarks

We have used the Argo data set to obtain the mean values and long-term variability of the vertical structure of the water column and the transports in and out of the Scotia Sea. In particular, we have provided estimates of the water balances for water masses that are fully sampled by the floats (SASW, SAMW, AASW/AAIW, UCDW), in our case down to the 28.0 kg m^{-3} isoneutral surface. Additionally, the Argo data set has delivered information on the main pathways along the 1,000 m parking depth.

The Argo floats data set is already large enough to assess the interannual and seasonal variability of the water transports down to the 28.0 kg m^{-3} isoneutral in the Drake and Northern Passages (Figures 13, 15, and 17). Regarding interannual variability, we have grouped the data over 5 yr periods in order to have a robust result, although this discards the possibility of detecting any signal with shorter periods. With respect to seasonal variability, we have selected 3 months averaging as this is the longest possible interval to detect the seasonal cycle; the results over three months are somewhat noisy but do demonstrate the presence of substantial seasonality in the transports.

The 3 months averages show that the water transports (down to $\gamma^n = 28.0$ kg m^{-3}) range between 110.8 and 174.5 Sv for the Drake Passage and between 101.9 and 135.3 Sv for the Northern Passages (Figure 17a). The mean transport is 149.9 ± 20.2 Sv through the Drake Passage and 122.1 ± 10.0 Sv through the Northern Passages; the mean and SD of the imbalance is 27.8 ± 24.0 Sv. The correlation between the Drake and northern transports peaks at 0.79 for time lags of 6.4 months (significant at $p < 0.01$). This time lag is one month shorter than the mean residence time of water masses in the Scotia Sea (219 days or 7.3 months), as deduced from the time that Argo floats take to cross it.

Considering the 5 yr values, the water transports (down to $\gamma^n = 28.0$ kg m^{-3}) range between 145.8 and 167.7 Sv in the Drake Passage and between 111.1 and 137.6 Sv in the Northern Passages (Figure 17b). The

intermediate and upper-circumpolar water masses display similar large variability, with a remarkable decrease in the intermediate layers and increase in the upper-circumpolar waters during the last years of the time series (2014–2016). The mean and SD transports are 156.8 ± 7.4 Sv through the Drake Passage and 122.4 ± 8.3 Sv through the Northern Passages; the mean and SD of the imbalance is 34.4 ± 13.9 Sv.

Considering the transports down to 28.0 kg m^{-3}, the mean values obtained using the entire data set (140.8 Sv through the Drake Passage and 115.9 Sv through the Northern Passages) are slightly below the mean values from either the 5 yr ensembles (156.8 and 122.4 Sv, respectively) or the 3 months groups (149.9 and 122.1 Sv, respectively). These differences possibly arise because the seasonal and interannual oscillations are not sinusoidal and, further, because the 5 yr average give less relative weight to the initial and final years of the time series (e.g., only one 5 yr value uses the 2018 data while five values use the 2012 data). Hence, we consider that our best mean transport estimates come from the full data set with the SD from the 5 yr periods (140.8 ± 7.4 Sv for the Drake Passage and 115.9 ± 8.3 Sv for the Northern Passages).

The SD of the total transports through the Drake and Northern Passages is generally smaller than the SD of either the baroclinic or barotropic contributions (Table 6). The 5 yr averaged time series of the baroclinic and barotropic contributions display much greater variations than the joint transport (Figures 17 and S5, Supporting Information). The two portions tend to compensate each other: for the Drake Passage, between 2011 and 2016 the baroclinic transport increased at the expense of the barotropic one, with a similar occurrence between 2010 and 2014 in the Northern Passages. This observation raises the possibility of interannual frontogenesis in the upper 2,000 m accompanied by a weakening of the currents at depth; such an effect is also suggested by the observed interannual changes in the shares of the surface-intermediate vs. upper-circumpolar waters (Figure 13).

Naveira Garabato et al. (2003) and Smith et al. (2010) suggested that there is substantial exchange of water masses across the PF and SAF in the North Scotia Ridge, leading to water transformations from deep to intermediate layers. Smith et al. (2010) determined that there is a total net transfer of 37 Sv from the PF to the SAF, with about 10 Sv corresponding to the AASW/AAIW masses. Our results, obtained following a different approach, are consistent with this view. Setting the fronts location at 1,000 m as the boundaries between the water masses, we have explored the transports and number of floats that transit between adjacent fronts, down to the 28.0 kg m^{-3} isoneutral surface. The dominance of the relatively warm input (at the Drake Passage the transports north and south of the PF are 101.3 and 39.6 Sv, respectively) contrasts with the preponderance of the relatively cold outputs (in the Northern Passages, we find 45.4 and 70.5 Sv to the west and east of the PF, respectively). Similarly, the difference between floats entering north and south of the PF location at 1,000 m (141 and 46) and exiting west and east of the PF (99 and 88) is remarkable.

We also observe some interannual variability in the intensity and position of both the SAF and, particularly, the PF across the Drake Passage (Figure 12). This is consistent with previous reports of a bimodal character of the PF (Cunningham et al., 2003; Lenn et al., 2007; Sprintall, 2003). Along the North Scotia Ridge, the SAF is always located in the 54–54 Passage while the PF is found in the western margin of the Shag Rocks Passage. The jets associated with these fronts are rather localized, yet their intensity displays substantial interannual variability, which leads to the observed changes in transport (Figures 13 and 17).

There is low seasonal variability associated with the SAF and PF in the Drake Passage, which contrasts with the relatively high seasonal SD in the mode and intermediate waters between these fronts (Figure 14). The surface mode waters experience seasonal changes in density and velocity that translate in a decrease of the transport of mode and intermediate waters (Figure 15). The large variations in the density structure and water transports in the Northern Passages support the idea of substantial seasonal changes in the transit time through the Scotia Sea (Figure 17).

Note that the observed seasonal and interannual variability in the frontal structures takes place mostly in the surface and intermediate waters, typically much shallower than the 1,000 m parking depth we have used to locate the frontal systems (Figure S1, Supporting Information). This is a source of uncertainty in the computed exchanges of water transports among frontal domains, which suggest that water transformations may be somewhat smaller than computed. Nevertheless, the observed high exchange of floats between frontal domains proves that most of the water changes are indeed real.

The Argo data set proves to be a very useful resource to improve our knowledge of the hydrographic variables and reference velocities, both of the mean fields and their spatiotemporal variability, in remote regions such as the Scotia Sea. Further, the data set complements the Eulerian averages with a Lagrangian view of those spatial connections that lie behind the variability. As the amount of available data increases, further analyses of the Argo data set shall be able to improve this emerging image.

Conflict of Interest

The authors declare no conflicts of interest relevant to this study.

Data Availability Statement

Argo float casts and positions are available from http://www.coriolis.eu.org, the float metadata and parking depths come from https://www.usgodae.org/cgi-bin/argo_select.pl and the NOAA and L.M. Gould SADCP data sets are obtained from https://accession.nodc.noaa.gov/NCEI-UH-JASADCP and http://adcp.ucsd.edu/lmgould/, respectively.

Acknowledgments
This work has been funded by the Spanish Government through project SAGA (Ministerio de Ciencia, Innovación y Universidades, ref. no. RTI2018-100844-B-C33). AOA is grateful to the FPU program, funded by the Spanish Government (Ministerio de Educación, Cultura y Deporte, reference FPU17/03796). The authors wish to acknowledge the International Argo Program, the contributing national programs that are part of the Global Ocean Observing System, and the Coriolis website that collects and distributed the data. The authors are very grateful to our editor, Laurence Padman, and an anonymous reviewer for providing many useful comments and suggestions. The authors are also grateful to Chad Greene for making available software and data for the Southern Ocean Database. This article is a publication of the Unidad Océano y Clima of the Universidad de Las Palmas de Gran Canaria, a R+D+I CSIC-associate unit. The authors also recognize the institutional support of the Spanish Government through the Severo Ochoa Center of Excellence accreditation (CEX2019-000928-S).

References

Arhan, M., Heywood, K. J., & King, B. A. (1999). The deep waters from the Southern Ocean at the entry to the Argentine Basin. *Deep-Sea Research II*, *46*, 475–499. https://doi.org/10.1016/s0967-0645(98)00110-6

Caldwell, P. C., Firing, E., & Hummon, J. M. (2010). *Ocean currents measured by Shipboard Acoustic Doppler Current Profilers (SADCP) from global oceans as part of the Joint Archive (JASADCP) since 1985. Southern Ocean, Scotia Sea, Ross Sea Data set*. NOAA National Centers for Environmental Information. Accessed December 2020.

Chidichimo, M. P., Donohue, K. A., Watts, D. R., & Tracey, K. L. (2014). Baroclinic transport time series of the Antarctic Circumpolar Current measured in Drake Passage. *Journal of Physical Oceanography*, *44*(7), 1829–1853. https://doi.org/10.1175/jpo-d-13-071.1

Colin de Verdière, A., & Ollitrault, M. (2016). A direct determination of the World Ocean Barotropic circulation. *Journal of Physical Oceanography*, *46*(1), 255–273. https://doi.org/10.1175/jpo-d-15-0046.1

Cunningham, S. A., Alderson, S. G., King, B. A., & Brandon, M. A. (2003). Transport and variability of the Antarctic Circumpolar Current in Drake Passage. *Journal of Geophysical Research: Oceans*, *108*(C5), 8084. https://doi.org/10.1029/2001jc001147

Donohue, K. A., Tracey, K. L., Watts, D. R., Chidichimo, M. P., & Chereskin, T. K. (2016). Mean Antarctic Circumpolar Current transport measured in Drake Passage. *Geophysical Research Letters*, *43*(22), 11760–11767. https://doi.org/10.1002/2016gl070319

Firing, Y. L., Chereskin, T. K., & Mazloff, M. R. (2011). Vertical structure and transport of the Antarctic Circumpolar Current in Drake Passage from direct velocity observations. *Journal of Geophysical Research: Oceans*, *116*(C8). https://doi.org/10.1029/2011jc006999

Ganachaud, A., & Wunsch, C. (2000). Improved estimates of global ocean circulation, heat transport and mixing from hydrographic data. *Nature*, *408*, 453–457, https://doi.org/10.1038/35044048

Gille, S. (2003). Float observations of the Southern Ocean. Part I: Estimating mean fields, bottom velocities, and topographic steering. *Journal of Physical Oceanography* , *33*, 1167–1181, https://doi.org/10.1175/1520-0485(2003)033<1167:footso>2.0.co;2

Gille, S., Josey, S., & Swart, S. (2016). New approaches for air-sea fluxes in the Southern Ocean. *Eos*, *97*. https://doi.org/10.1029/2016EO052243

Greene, C. (2020). *SODB Southern Ocean Database Toolbox*. MATLAB Central File Exchange Retrieved from https://www.mathworks.com/matlabcentral/fileexchange/52347-sodb-southern-ocean-database-toolbox

Kim, Y. S., & Orsi, A. H. (2014). On the variability of Antarctic Circumpolar Current fronts inferred from 1992–2011 Altimetry. *Journal of Physical Oceanography*, *44*(12), 3054–3071. https://doi.org/10.1175/jpo-d-13-0217.1

Koenig, Z., Provost, C., Ferrari, R., Sennéchael, N., & Rio, M. H. (2014). Volume transport of the Antarctic Circumpolar Current: Production and validation of a 20 year long time series obtained from in situ and satellite observations. *Journal of Geophysical Research: Oceans*, *119*(8), 5407–5433. https://doi.org/10.1002/2014jc009966

Lebedev, K. V., Yoshinari, H., Maximenko, N. A., & Hacker, P. W. (2007). YoMaHa'07: Velocity data assessed from trajectories of Argo floats at parking level and at the sea surface. *IPRC Technical Note*, *4*(2), 1–16. https://doi.org/10.2205/2007es000283

Lenn, Y.-D., Chereskin, T. K., Sprintall, J., & Firing, E. (2007). Mean jets, mesoscale variability and eddy momentum fluxes in the surface layer of the Antarctic Circumpolar Current in Drake Passage. *Journal of Marine Research*, *65*(1), 27–58. https://doi.org/10.1357/002224007780388694

Liu, J., & Curry, J. A. (2010). Accelerated warming of the Southern Ocean and its impacts on the hydrological cycle and sea ice. *Proceedings of the National Academy of Sciences*, *107*(34), 14987–14992. https://doi.org/10.1073/pnas.1003336107

Locarnini, R. A., Whitworth, T., & Nowlin, W. D. (1993). The importance of the Scotia Sea on the outflow of Weddell Sea Deep Water. *Journal of Marine Research*, *51*(1), 135–153. https://doi.org/10.1357/0022240933223846

Meredith, M. P. (2003). Southern ACC front to the northeast of South Georgia: Pathways, characteristics, and fluxes. *Journal of Geophysical Research*, *108*(C5), 3162. https://doi.org/10.1029/2001JC001227

Naveira Garabato, A. C., Heywood, K. J., & Stevens, D. P. (2002). Modification and pathways of Southern Ocean Deep Waters in the Scotia Sea. *Deep-Sea Research Part I Oceanographic Research Papers*, *49*(4), 681–705. https://doi.org/10.1016/S0967-0637(01)00071-1

Naveira Garabato, A. C., Stevens, D. P., & Heywood, K. J. (2003). Water mass conversion, fluxes and mixing in the Scotia Sea diagnosed by an inverse model. *Journal of Physical Oceanography*, *33*, 2565–2587. https://doi.org/10.1175/1520-0485(2003)033<2565:wmcfam>2.0.co;2

Ollitrault, M., & Rannou, J. P. (2013). ANDRO: An Argo-based deep displacement dataset. *Journal of Atmospheric and Oceanic Technology*, *30*(4), 759–788. https://doi.org/10.1175/jtech-d-12-00073.1

Orsi, A. H., & Whitworth, T., III. (2005). In M. Sparrow, P. Chapman, & J. Gould (Eds.), *Hydrographic Atlas of the World Ocean Circulation Experiment (WOCE). Volume 1: Southern Ocean*. International WOCE Project Office.

Orsi, A. H., Whitworth, T., & Nowlin, W. D. (1995). On the meridional extent and fronts of the Antarctic Circumpolar Current. *Deep-Sea Research Part I*, *42*(5), 641–673. https://doi.org/10.1016/0967-0637(95)00021-w

Palmer, M., Gomis, D., del Mar Flexas, M., Jordà, G., Jullion, L., Tsubouchi, T., & Garabato, A. C. N. (2012). Water mass pathways and transports over the South Scotia Ridge west of 50°W. *Deep Sea Research Part I: Oceanographic Research Papers*, *59*, 8–24. https://doi.org/10.1016/j.dsr.2011.10.005

Reid, J. L., Nowlin, W. D., Jr, & Patzert, W. C. (1977). On the characteristics and circulation of the southwestern Atlantic Ocean. *Journal of Physical Oceanography*(7), 62–91. https://doi.org/10.1175/1520-0485(1977)007<0062:otcaco>2.0.co;2

Rintoul, S. R., & Naveira Garabato, A. C. (2013). Dynamics of the Southern Ocean circulation. *International Geophysics*, *103*, 471–492. https://doi.org/10.1016/b978-0-12-391851-2.00018-0

Rosell-Fieschi, M., Pelegrí, J. L., & Gourrion, J. (2015). Zonal jets in the equatorial Atlantic Ocean. *Progress in Oceanography*, *130*, 1–18. https://doi.org/10.1016/j.pocean.2014.08.008

Sievers, H. A., & Nowlin, W. D., Jr. (1984). The stratification and water masses at Drake Passage. *Journal of Geophysical Research*, *89*, 10489–10514. https://doi.org/10.1029/jc089ic06p10489

Sloyan, B. M., & Rintoul, S. R. (2001). Circulation, renewal, and modification of Antarctic Mode Water and Intermediate Water. *Journal of Physical Oceanography*, *31*, 1005–1030, https://doi.org/10.1175/1520-0485(2001)031<1005:cramoa>2.0.co;2

Smith, I. J., Stevens, D. P., Heywood, K. J., & Meredith, M. P. (2010). The flow of the Antarctic Circumpolar Current over the North Scotia Ridge. *Deep-Sea Research Part I: Oceanographic Research Papers*, *57*(1), 14–28. https://doi.org/10.1016/j.dsr.2009.10.010

Sokolov, S., & Rintoul, S. R. (2007). Multiple Jets of the Antarctic Circumpolar Current South of Australia. *Journal of Physical Oceanography*, *37*(5), 1394–1412. https://doi.org/10.1175/jpo3111.1

Sokolov, S., & Rintoul, S. R. (2009a). Circumpolar structure and distribution of the Antarctic Circumpolar Current fronts: 1. Mean circumpolar paths. *Journal of Geophysical Research*, *114*, C11018. https://doi.org/10.1029/2008JC005108

Sokolov, S., & Rintoul, S. R. (2009b). Circumpolar structure and distribution of the Antarctic Circumpolar Current fronts: 2. Variability and relationship to sea surface height. *Journal of Geophysical Research: Oceans*, *114*(C11). https://doi.org/10.1029/2008jc005248

Sprintall, J. (2003). Seasonal to interannual upper-ocean variability in the Drake Passage. *Journal of Marine Research*, *61*(1), 27–57. https://doi.org/10.1357/002224003321586408

Thompson, A. F., & Sallée, J. B. (2012). Jets and topography: Jet transitions and the impact on transport in the Antarctic Circumpolar Current. *Journal of Physical Oceanography*, *42*(6), 956–972. https://doi.org/10.1175/jpo-d-11-0135.1

Thorpe, S. E., Heywood, K. J., Brandon, M. A., & Stevens, D. P. (2002). Variability of the southern Antarctic Circumpolar Current front north of South Georgia. *Journal of Marine Systems*, *37*(1–3), 87–105. https://doi.org/10.1016/S0924-7963(02)00197-5

Van Den Broeke, M. R., & Van Lipzig, N. P. (2004). Changes in Antarctic temperature, wind, and precipitation in response to the Antarctic Oscillation. *Annals of Glaciology*, *39*, 119–126. https://doi.org/10.3189/172756404781814654

Whitworth, T., III, Nowlin, W. D., Jr., & Worley, S. J. (1982). The net transport of the Antarctic Circumpolar Current through Drake Passage. *Journal of Physical Oceanography*, *12*(9), 960–971. https://doi.org/10.1175/1520-0485(1982)012<0960:tntota>2.0.co;2

Whitworth, T., & Peterson, R. G. (1985). Volume transport of the Antarctic Circumpolar Current from bottom pressure measurements. *Journal of Physical Oceanography*, *15*, 810–816. https://doi.org/10.1175/1520-0485(1985)015<0810:vtotac>2.0.co;2

Yoshinari, H., Maximenko, N. A., & Hacker, P. W. (2006). YoMaHa'05: Velocity data assessed from trajectories of Argo floats at parking level and at the sea surface. *IPRC Technical Note*, *4*, 20.